Universität Karlsruhe (TH)
Institut für Baustatik

Structural analysis of composite laminates using a mixed hybrid shell element

F. Gruttmann, W. Wagner

Mitteilung 2(2005)

Universität Karlsruhe (TH)
Institut für Baustatik

Structural analysis of composite laminates using a mixed hybrid shell element

F. Gruttmann, W. Wagner

Mitteilung 2(2005)

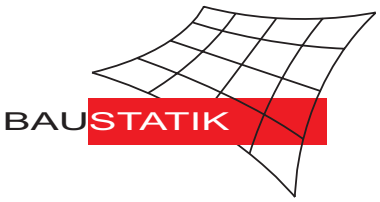

Prof. Dr.–Ing. W. Wagner
Institut für Baustatik
Universität Karlsruhe
Postfach 6980
76128 Karlsruhe

Telefon: (0721) 608–2280
Telefax: (0721) 608–6015
E–mail: bs@.uni-karlsruhe.de
Internet: http://www.bs.uni-karlsruhe.de

Structural analysis of composite laminates using a mixed hybrid shell element

Friedrich Gruttmann and Werner Wagner

Friedrich Gruttmann
Institut für Werkstoffe und Mechanik im Bauwesen
Technische Universität Darmstadt
Petersenstraße 12
64287 Darmstadt, Germany
Tel.: +49-6151-16-2537
Fax: +49-6151-16-2538
Email: Gruttmann@iwmb.tu-darmstadt.de

Werner Wagner
Institut für Baustatik
Universität Karlsruhe (TH)
Kaiserstraße 12
76131 Karlsruhe, Germany
Tel.: +49-721-608-2280
Fax: +49-721-608-6015
Email: ww@bs.uka.de

Abstract The structural analysis of thin composite structures requires robust and effective shell elements. In this paper the variational formulation is based on a Hu–Washizu functional with independent displacements, stress resultants and shell strains. For the independent shell strains an enhanced interpolation part is introduced. This yields an improved convergence behaviour especially for laminated shells with coupled membrane and bending stiffness. The developed mixed hybrid shell element possesses the correct rank and fulfills the in–plane and bending patch test. The formulation is tested by several nonlinear examples including bifurcation and post–buckling response. The essential feature of the new element is the robustness in nonlinear computations with large rigid body motions. It allows very large load steps in comparison to standard displacement models.

1 Introduction

The application of composite materials became very popular in the last decades, especially in aircraft industries. The advantages of these materials are high strength and stiffness ratios coupled with a low specific weight. Thus, composites are used in highly loaded light weight structures. Often the designed constructions are thin shells which are very sensitive against loss of stability. Therefore the discussion of the stability behaviour is crucial for composite shell problems besides the description of material phenomena like matrix and fiber cracking or delamination, see e.g. Ref. [1]. Thus high requirements on the accuracy and robustness of the finite element models are essential.

Computational shell analysis is based on a stress resultant theory e.g. Ref. [2], or on the so–called degenerated approach, References [3, 4]. Although the hypotheses underlying the classical shell theory and degenerated approach are essentially the same, the reduction to resultant form is typically carried out analytically in the former, and numerically in the latter. Many of the computational shell models consider transverse shear deformations within a Reissner–Mindlin theory to by–pass the difficulties caused by C^1–requirements of the Kirchhoff–Love theory. Low order elements based on a standard displacement interpolation are usually characterized by locking phenomena and thus lead to unacceptable stiff results when reasonable finite element meshes are employed. In shells two types of locking occur: transverse shear locking in which bending modes are excluded and nearly all energy is stored in transverse

shear terms, and membrane locking in which all bending energy is restrained and energy is stored in membrane terms. In attempting to avoid locking, reduced integration methods have been advocated, Ref. [5]. Use of reduced (or selective reduced) integration is often accompanied by spurious zero energy modes. Hence, authors have developed stabilization techniques to regain the correct rank of the element stiffness matrix, e.g. References [6, 7, 8].
In case of linear elasticity the Hellinger–Reissner functional can be used as variational basis for mixed interpolated elements. For nonlinear material behaviour a three field Hu–Washizu functional with independent displacements, stresses and strains is more appropriate. Within the so–called enhanced strain formulations the independent stresses are eliminated from the set of equations using orthogonality conditions and a two field formulation remains, Ref. [9]. For shells this method has been applied enhancing the Green–Lagrangean membrane strains e.g. in Ref. [10]. An effective method to avoid transverse shear locking is based on assumed shear strain fields first proposed in Ref. [11], and subsequently extended among others in References [12, 13, 14]. The variational basis for these methods is given with the Hu–Washizu functional.
An important issue within the context of developing a finite shell model is the number and type of rotation parameters on the element. Mostly general shell theories exclude explicit dependence of a rotational field about the normal to the shell surface which leads to a five parameter model (three displacements and two local rotations). Use of 5 degree–of–freedom frame requires construction of special coordinate systems for the rotational parameters. Considering the so–called drilling degree-of–freedom leads to a finite element discretization with six nodal parameters. This has some advantages since both displacement and rotation parameters are associated with a global coordinate frame. On the other hand a larger set of algebraic equations has to be solved, e.g. Ref. [15].

The new aspects and essential features of the present formulation are as follows:

(i) The nonlinear variational formulation is based on a Hu–Washizu functional using a material representation with independent displacements, stresses and strains. The associated Euler–Lagrange equations are the static and geometric field equations, the constitutive equations and the static boundary conditions. The kinematic relations account for transverse shear deformations and are valid for finite rotations. In this paper the strain energy is chosen as a quadratic function of the independent shell strains. Based on a previous publication [16], where appropriate interpolation functions for the independent stress resultants and strains are formulated, we present several new theoretical developments.

(ii) In this paper the strain approximation is modified. The first part with 14 parameters corresponds to the stress interpolation. The second part with a variable number or parameters is chosen orthogonal to the stress shape functions. This procedure corresponds to the enhanced strain formulation, Ref. [9]. As result the derived mixed hybrid quadrilateral element fulfills the membrane and bending patch test and possesses the correct rank.

(iii) It is shown that the second part of the strain interpolation leads to an improvement of the element behaviour especially when coupling of the membrane and bending stiffness occurs. This is the case for laminated shells with certain layer sequences. For this

purpose the material matrix for laminates assuming transversal isotropic behaviour for each layer is implemented. An effective procedure to eliminate the stress and strain parameters on the element level to avoid expensive matrix inversions is developed.

(iv) The element formulation allows the analysis of shells with intersections. The nodal degrees of freedom are: three global displacement components, three global rotations at nodes on intersections and two local rotations at other nodes.

(v) The developed element is tested at several shell problems. We investigate the nonlinear behaviour of thin laminated structures including stability. The essential feature of the new element is the robustness in nonlinear computations with large rigid body motions. It allows very large load steps and needs less iterations in comparison to other element formulations.

2 Hu–Washizu variational formulation

Let $\mathcal{B}$ be the three–dimensional Euclidean space occupied by the shell in the reference configuration. With ξ^i and $\mathbf{e}_i$ we denote a convected coordinate system of the body and the global cartesian basis system, respectively. The coordinate ξ^3 is bounded by $h_u \leq \xi^3 \leq h_0$ and $\xi^3 = 0$ defines the arbitrary reference surface Ω. A director vector $\mathbf{D}(\xi^1, \xi^2)$ with $|\mathbf{D}(\xi^1, \xi^2)| = 1$ is defined as a vector perpendicular to Ω. The unit director $\mathbf{d}$ of the current configuration is obtained by an orthogonal transformation of the initial vector $\mathbf{D}$. In the following the summation convention is used for repeated indices, where Latin indices range from 1 to 3 and Greek indices range from 1 to 2. Commas denote partial differentiation with respect to the coordinates ξ^α.
The shell is loaded statically by surface loads $\bar{\mathbf{p}}$ on Ω and by boundary loads $\bar{\mathbf{t}}$ on the boundary Γ_σ. Hence the basic Hu–Washizu functional is introduced

$$\Pi(\mathbf{v}, \boldsymbol{\sigma}, \boldsymbol{\varepsilon}) = \int_{(\Omega)} [W(\boldsymbol{\varepsilon}) + \boldsymbol{\sigma}^T(\boldsymbol{\varepsilon}_G(\mathbf{v}) - \boldsymbol{\varepsilon})]\, dA - \int_{(\Omega)} \mathbf{u}^T \bar{\mathbf{p}}\, dA - \int_{(\Gamma_\sigma)} \mathbf{u}^T\, \bar{\mathbf{t}}\, ds \rightarrow \text{stat.} \tag{1}$$

with the area element of the shell $dA = j\, d\xi^1\, d\xi^2$ where $j = |\mathbf{X}_{,1} \times \mathbf{X}_{,2}|$. Here, $\mathbf{v} = [\mathbf{u}, \boldsymbol{\omega}]^T$, $\boldsymbol{\varepsilon}$, and $\boldsymbol{\sigma}$ denote the independent displacement, strain and stress fields. The displacement vector of the reference surface follows from $\mathbf{u} = \mathbf{x} - \mathbf{X}$, where $\mathbf{X}(\xi^1, \xi^2)$ and $\mathbf{x}(\xi^1, \xi^2)$ denote the position vectors of the initial and current shell reference surface. Furthermore $\boldsymbol{\omega}$ is the vector of rotational parameters. In this paper we assume a strain energy W which is a quadratic function of the independent strains.
The shell strains based on a Reissner–Mindlin kinematic are organized in a vector

$$\boldsymbol{\varepsilon}_G(\mathbf{v}) = [\varepsilon_{11}, \varepsilon_{22}, 2\varepsilon_{12}, \kappa_{11}, \kappa_{22}, 2\kappa_{12}, \gamma_1, \gamma_2]^T, \tag{2}$$

where the membrane strains $\varepsilon_{\alpha\beta}$, curvatures $\kappa_{\alpha\beta}$ and shear strains γ_α can be derived from the Green-Lagrangean strain tensor

$$\begin{aligned} \varepsilon_{\alpha\beta} &= \frac{1}{2}(\mathbf{x}_{,\alpha} \cdot \mathbf{x}_{,\beta} - \mathbf{X}_{,\alpha} \cdot \mathbf{X}_{,\beta}) \\ \kappa_{\alpha\beta} &= \frac{1}{2}(\mathbf{x}_{,\alpha} \cdot \mathbf{d}_{,\beta} + \mathbf{x}_{,\beta} \cdot \mathbf{d}_{,\alpha} - \mathbf{X}_{,\alpha} \cdot \mathbf{D}_{,\beta} - \mathbf{X}_{,\beta} \cdot \mathbf{D}_{,\alpha}) \\ \gamma_\alpha &= \mathbf{x}_{,\alpha} \cdot \mathbf{d} - \mathbf{X}_{,\alpha} \cdot \mathbf{D} \end{aligned} \tag{3}$$

The work conjugate stress resultants are integrals of the Second Piola–Kirchhoff stress tensor

$$\boldsymbol{\sigma} = [n^{11}, n^{22}, n^{12}, m^{11}, m^{22}, m^{12}, q^1, q^2]^T \tag{4}$$

with membrane forces $n^{\alpha\beta} = n^{\beta\alpha}$, bending moments $m^{\alpha\beta} = m^{\beta\alpha}$ and shear forces q^α.

Introducing $\boldsymbol{\theta} := [\mathbf{v}, \boldsymbol{\sigma}, \boldsymbol{\varepsilon}]^T$ and $\delta\boldsymbol{\theta} := [\delta\mathbf{v}, \delta\boldsymbol{\sigma}, \delta\boldsymbol{\varepsilon}]^T$ the stationary condition reads

$$\begin{aligned} \delta\Pi \;:=\; g(\boldsymbol{\theta}, \delta\boldsymbol{\theta}) = & \int_{(\Omega)} [\delta\boldsymbol{\varepsilon}^T(\partial_{\boldsymbol{\varepsilon}} W - \boldsymbol{\sigma}) + \delta\boldsymbol{\sigma}^T(\boldsymbol{\varepsilon}_G - \boldsymbol{\varepsilon}) + \delta\boldsymbol{\varepsilon}_G^T\boldsymbol{\sigma}]\, dA \\ & - \int_{(\Omega)} \delta\mathbf{u}^T \bar{\mathbf{p}}\, dA - \int_{(\Gamma_\sigma)} \delta\mathbf{u}^T\, \bar{\mathbf{t}}\, ds = 0 \end{aligned} \tag{5}$$

with the virtual shell strains $\delta\boldsymbol{\varepsilon}_G = [\delta\varepsilon_{11}, \delta\varepsilon_{22}, 2\delta\varepsilon_{12}, \delta\kappa_{11}, \delta\kappa_{22}, 2\delta\kappa_{12}, \delta\gamma_1, \delta\gamma_2]^T$

$$\begin{aligned} \delta\varepsilon_{\alpha\beta} &= \frac{1}{2}(\delta\mathbf{x}_{,\alpha}\cdot\mathbf{x}_{,\beta} + \delta\mathbf{x}_{,\beta}\cdot\mathbf{x}_{,\alpha}) \\ \delta\kappa_{\alpha\beta} &= \frac{1}{2}(\delta\mathbf{x}_{,\alpha}\cdot\mathbf{d}_{,\beta} + \delta\mathbf{x}_{,\beta}\cdot\mathbf{d}_{,\alpha} + \delta\mathbf{d}_{,\alpha}\cdot\mathbf{x}_{,\beta} + \delta\mathbf{d}_{,\beta}\cdot\mathbf{x}_{,\alpha}) \\ \delta\gamma_\alpha &= \delta\mathbf{x}_{,\alpha}\cdot\mathbf{d} + \delta\mathbf{d}\cdot\mathbf{x}_{,\alpha}\ . \end{aligned} \tag{6}$$

With integration by parts and applying standard arguments of variational calculus one obtains the associated Euler–Lagrange equations

$$\left.\begin{aligned} \tfrac{1}{j}(j\,\mathbf{n}^\alpha)_{,\alpha} + \bar{\mathbf{p}} &= \mathbf{0} & \qquad \boldsymbol{\varepsilon}_G - \boldsymbol{\varepsilon} &= \mathbf{0} \\ \tfrac{1}{j}(j\,\mathbf{m}^\alpha)_{,\alpha} + \mathbf{x}_{,\alpha}\times\mathbf{n}^\alpha &= \mathbf{0} & \qquad \partial_{\boldsymbol{\varepsilon}} W - \boldsymbol{\sigma} &= \mathbf{0} \end{aligned}\right\} \quad \text{in } \Omega \tag{7}$$

with $\mathbf{n}^\alpha := n^{\alpha\beta}\,\mathbf{x}_{,\beta} + q^\alpha\,\mathbf{d} + m^{\alpha\beta}\,\mathbf{d}_{,\beta}$ and $\mathbf{m}^\alpha := \mathbf{d}\times m^{\alpha\beta}\,\mathbf{x}_{,\beta}$. The principle yields the static field equations with local form of linear and angular momentum, the geometric field equations and the constitutive equations. Furthermore the static boundary conditions $\mathbf{t} - \bar{\mathbf{t}} = \mathbf{0}$ on Γ_σ with $\mathbf{t}$ the boundary forces related to $\mathbf{n}^\alpha$ follow. Finally, the geometric boundary conditions $\mathbf{u} - \bar{\mathbf{u}} = \mathbf{0}$ on Γ_u have to be fulfilled as constraints.

3 Finite Element Equations

3.1 Interpolation of the initial and current reference surface

In this section the finite element equations for quadrilaterals are specified applying the isoparametric concept. The local numbering of the corner nodes and midside node can be seen in Fig. 1.

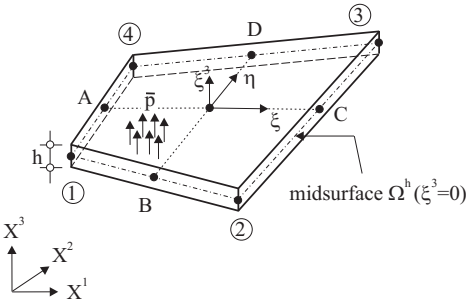

Figure 1: Quadrilateral shell element

A map of the coordinates $\{\xi, \eta\} \in [-1, 1]$ from the unit square to the midsurface in the initial and current configuration is applied. Thus the position vector and the director vector of the reference surface are interpolated with bi–linear functions

$$\mathbf{X}^h = \sum_{I=1}^{4} N_I \, \mathbf{X}_I \qquad \mathbf{D}^h = \sum_{I=1}^{4} N_I \, \mathbf{D}_I \qquad N_I = \frac{1}{4}(1 + \xi_I \xi)(1 + \eta_I \eta) \tag{8}$$

with $\xi_I \in \{-1, \quad 1, \quad 1, -1\}$ and $\eta_I \in \{-1, -1, \quad 1, \quad 1\}$. The superscript h denotes the characteristic size of the element discretization and indicates the finite element approximation. The nodal position vectors $\mathbf{X}_I$ and the local cartesian basis systems $[\mathbf{A}_{1I}, \mathbf{A}_{2I}, \mathbf{A}_{3I}]$ are generated within the mesh input. Here, $\mathbf{D}_I = \mathbf{A}_{3I}$ is perpendicular to Ω and $\mathbf{A}_{1I}$, $\mathbf{A}_{2I}$ are constructed in such a way that the boundary conditions can be accommodated. With $(8)_2$ the orthogonality is only given at the nodes.
For each element a local cartesian basis $\mathbf{t}_i$ is evaluated

$$\begin{aligned}
\bar{\mathbf{d}}_1 &= \mathbf{X}_3 - \mathbf{X}_1 & \widehat{\mathbf{d}}_{\mathbf{1}} &= \bar{\mathbf{d}}_1 / |\bar{\mathbf{d}}_1| \\
\bar{\mathbf{d}}_2 &= \mathbf{X}_2 - \mathbf{X}_4 & \widehat{\mathbf{d}}_{\mathbf{2}} &= \bar{\mathbf{d}}_2 / |\bar{\mathbf{d}}_2| \\
\mathbf{t}_1 &= (\widehat{\mathbf{d}}_{\mathbf{1}} + \widehat{\mathbf{d}}_{\mathbf{2}}) / |\widehat{\mathbf{d}}_{\mathbf{1}} + \widehat{\mathbf{d}}_{\mathbf{2}}| \\
\mathbf{t}_2 &= (\widehat{\mathbf{d}}_{\mathbf{1}} - \widehat{\mathbf{d}}_{\mathbf{2}}) / |\widehat{\mathbf{d}}_{\mathbf{1}} - \widehat{\mathbf{d}}_{\mathbf{2}}| \\
\mathbf{t}_3 &= \mathbf{t}_1 \times \mathbf{t}_2 \, .
\end{aligned} \tag{9}$$

One could also use the so-called lamina basis according to Ref. [17], where the base vectors $\mathbf{t}_\alpha$ lie as close as possible to the coordinates ξ and η. Hence the Jacobian matrix $\mathbf{J}$ is defined

$$\mathbf{J} = \begin{bmatrix} \mathbf{X}^h_{,\xi} \cdot \mathbf{t}_1 & \mathbf{X}^h_{,\xi} \cdot \mathbf{t}_2 \\ \mathbf{X}^h_{,\eta} \cdot \mathbf{t}_1 & \mathbf{X}^h_{,\eta} \cdot \mathbf{t}_2 \end{bmatrix} \tag{10}$$

with

$$\begin{aligned}
\mathbf{X}^h_{,\xi} &= \mathbf{G}^0_\xi + \eta \, \mathbf{G}^1 & \mathbf{G}^0_\xi &= \frac{1}{4} \sum_{I=1}^{4} \xi_I \, \mathbf{X}_I \\
\mathbf{X}^h_{,\eta} &= \mathbf{G}^0_\eta + \xi \, \mathbf{G}^1 & \mathbf{G}^0_\eta &= \frac{1}{4} \sum_{I=1}^{4} \eta_I \, \mathbf{X}_I \\
& & \mathbf{G}^1 &= \frac{1}{4} \sum_{I=1}^{4} \xi_I \, \eta_I \, \mathbf{X}_I \, .
\end{aligned} \tag{11}$$

One can prove that $\mathbf{t}_3 \cdot \mathbf{G}_\xi^0 = 0$ and $\mathbf{t}_3 \cdot \mathbf{G}_\eta^0 = 0$ holds which shows that $\mathbf{t}_3$ is normal vector at the element center. Thus $\mathbf{t}_1$ and $\mathbf{t}_2$ span a tangent plane at the center of the element. Now we are able to express the local cartesian derivatives of the shape functions using the inverse Jacobian matrix $\mathbf{J}$. The tangent vectors $\mathbf{X}_{,\alpha}$ and the derivatives of the director vector $\mathbf{D}_{,\alpha}$ are computed considering (8) as follows

$$\mathbf{X}^h_{,\alpha} = \sum_{I=1}^{4} N_{I,\alpha}\, \mathbf{X}_I \quad \mathbf{D}^h_{,\alpha} = \sum_{I=1}^{4} N_{I,\alpha}\, \mathbf{D}_I \quad \begin{bmatrix} N_{I,1} \\ N_{I,2} \end{bmatrix} = \mathbf{J}^{-1} \begin{bmatrix} N_{I,\xi} \\ N_{I,\eta} \end{bmatrix}. \tag{12}$$

For arbitrary warped elements one obtains $\mathbf{X}^h_{,\alpha} = \mathbf{t}_\alpha$ at the element center, which can be shown using above orthogonality conditions. This is important in the context of the present mixed interpolation. Furthermore a local cartesian system is advantageous to verify complicated nonlinear constitutive equations. At other points of the element the vectors $\mathbf{X}^h_{,\alpha}$ are only approximately orthogonal.

The current shell middle surface is approximated in the same way

$$\begin{aligned} \mathbf{x}^h &= \sum_{I=1}^{4} N_I\, \mathbf{x}_I & \qquad \mathbf{d}^h &= \sum_{I=1}^{4} N_I\, \mathbf{d}_I \\ \mathbf{x}^h_{,\alpha} &= \sum_{I=1}^{4} N_{I,\alpha}\, \mathbf{x}_I & \qquad \mathbf{d}^h_{,\alpha} &= \sum_{I=1}^{4} N_{I,\alpha}\, \mathbf{d}_I\,, \end{aligned} \tag{13}$$

where $\mathbf{x}_I = \mathbf{X}_I + \mathbf{u}_I$ describes the current nodal position vector and $\mathbf{d}_I = \mathbf{a}_{3I}$ is obtained by an orthogonal transformation $\mathbf{a}_{kI} = \mathbf{R}_I\, \mathbf{A}_{kI}, \quad k = 1, 2, 3$. The rotation tensor $\mathbf{R}_I$ is a function of the parameters ω_{kI} organized in the vector $\boldsymbol{\omega}_I = [\omega_{1I}, \omega_{2I}, \omega_{3I}]^T$ and is evaluated via Rodrigues' formula

$$\mathbf{R}_I = \mathbf{1} + \frac{\sin\omega_I}{\omega_I}\boldsymbol{\Omega}_I + \frac{1-\cos\omega_I}{\omega_I^2}\boldsymbol{\Omega}_I^2 \quad \boldsymbol{\Omega}_I = \operatorname{skew}\boldsymbol{\omega}_I = \begin{bmatrix} 0 & -\omega_{3I} & \omega_{2I} \\ \omega_{3I} & 0 & -\omega_{1I} \\ -\omega_{2I} & \omega_{1I} & 0 \end{bmatrix} \tag{14}$$

Representation (14) is singularity free for $\omega_I = |\boldsymbol{\omega}_I| < 2\pi$ which can always be fulfilled if after a certain number of load steps a multiplicative update of the total rotation tensor is applied.

The element has to fulfil membrane and bending patch test. The bending patch test – when using below defined mixed interpolation for the stress resultants and shell strains – can be fulfilled with substitute shear strains defined in Ref. [13], but not with the bilinear displacement interpolation inserted in the transverse shear strains $(3)_3$, see Ref. [18] in case of

a linear plate. Thus the finite element approximation of the Green–Lagrangean strains reads

$$\boldsymbol{\varepsilon}_G^h = \begin{bmatrix} \varepsilon_{11}^h \\ \varepsilon_{22}^h \\ 2\varepsilon_{12}^h \\ \kappa_{11}^h \\ \kappa_{22}^h \\ 2\kappa_{12}^h \\ \gamma_1^h \\ \gamma_2^h \end{bmatrix} = \begin{bmatrix} \frac{1}{2}\left(\mathbf{x}_{,1}^h \cdot \mathbf{x}_{,1}^h - \mathbf{X}_{,1}^h \cdot \mathbf{X}_{,1}^h\right) \\ \frac{1}{2}\left(\mathbf{x}_{,2}^h \cdot \mathbf{x}_{,2}^h - \mathbf{X}_{,2}^h \cdot \mathbf{X}_{,2}^h\right) \\ \mathbf{x}_{,1}^h \cdot \mathbf{x}_{,2}^h - \mathbf{X}_{,1}^h \cdot \mathbf{X}_{,2}^h \\ \mathbf{x}_{,1}^h \cdot \mathbf{d}_{,1}^h - \mathbf{X}_{,1}^h \cdot \mathbf{D}_{,1}^h \\ \mathbf{x}_{,2}^h \cdot \mathbf{d}_{,2}^h - \mathbf{X}_{,2}^h \cdot \mathbf{D}_{,2}^h \\ \mathbf{x}_{,1}^h \cdot \mathbf{d}_{,2}^h + \mathbf{x}_{,2}^h \cdot \mathbf{d}_{,1}^h - \mathbf{X}_{,1}^h \cdot \mathbf{D}_{,2}^h - \mathbf{X}_{,2}^h \cdot \mathbf{D}_{,1}^h \\ \mathbf{J}^{-1} \begin{Bmatrix} \frac{1}{2}[(1-\eta)\,\gamma_\xi^B + (1+\eta)\,\gamma_\xi^D \\ \frac{1}{2}[(1-\xi)\,\gamma_\eta^A + (1+\xi)\,\gamma_\eta^C] \end{Bmatrix} \end{bmatrix}. \tag{15}$$

The strains at the midside nodes A, B, C, D of the element are specified as follows

$$\begin{aligned} \gamma_\xi^M &= [\mathbf{x}_{,\xi} \cdot \mathbf{d} - \mathbf{X}_{,\xi} \cdot \mathbf{D}]^M \qquad & M &= B, D \\ \gamma_\eta^L &= [\mathbf{x}_{,\eta} \cdot \mathbf{d} - \mathbf{X}_{,\eta} \cdot \mathbf{D}]^L \qquad & L &= A, C\,, \end{aligned} \tag{16}$$

where the following quantities are given with the bilinear interpolation (8) and (13)

$$\begin{aligned} \mathbf{d}^A &= \tfrac{1}{2}(\mathbf{d}_4 + \mathbf{d}_1) & \mathbf{D}^A &= \tfrac{1}{2}(\mathbf{D}_4 + \mathbf{D}_1) \\ \mathbf{d}^B &= \tfrac{1}{2}(\mathbf{d}_1 + \mathbf{d}_2) & \mathbf{D}^B &= \tfrac{1}{2}(\mathbf{D}_1 + \mathbf{D}_2) \\ \mathbf{d}^C &= \tfrac{1}{2}(\mathbf{d}_2 + \mathbf{d}_3) & \mathbf{D}^C &= \tfrac{1}{2}(\mathbf{D}_2 + \mathbf{D}_3) \\ \mathbf{d}^D &= \tfrac{1}{2}(\mathbf{d}_3 + \mathbf{d}_4) & \mathbf{D}^D &= \tfrac{1}{2}(\mathbf{D}_3 + \mathbf{D}_4) \\ \mathbf{x}_{,\eta}^A &= \tfrac{1}{2}(\mathbf{x}_4 - \mathbf{x}_1) & \mathbf{X}_{,\eta}^A &= \tfrac{1}{2}(\mathbf{X}_4 - \mathbf{X}_1) \\ \mathbf{x}_{,\xi}^B &= \tfrac{1}{2}(\mathbf{x}_2 - \mathbf{x}_1) & \mathbf{X}_{,\xi}^B &= \tfrac{1}{2}(\mathbf{X}_2 - \mathbf{X}_1) \\ \mathbf{x}_{,\eta}^C &= \tfrac{1}{2}(\mathbf{x}_3 - \mathbf{x}_2) & \mathbf{X}_{,\eta}^C &= \tfrac{1}{2}(\mathbf{X}_3 - \mathbf{X}_2) \\ \mathbf{x}_{,\xi}^D &= \tfrac{1}{2}(\mathbf{x}_3 - \mathbf{x}_4) & \mathbf{X}_{,\xi}^D &= \tfrac{1}{2}(\mathbf{X}_3 - \mathbf{X}_4)\,. \end{aligned} \tag{17}$$

3.2 Interpolation of the stress resultants

The independent field of stress resultants $\boldsymbol{\sigma}$ is approximated as follows

$$\begin{aligned} \boldsymbol{\sigma}^h &= \mathbf{N}_\sigma\, \hat{\boldsymbol{\sigma}} & \mathbf{N}_\sigma &= \begin{bmatrix} \mathbf{1}_3 & \mathbf{0} & \mathbf{0} & \mathbf{N}_\sigma^m & \mathbf{0} & \mathbf{0} \\ \mathbf{0} & \mathbf{1}_3 & \mathbf{0} & \mathbf{0} & \mathbf{N}_\sigma^b & \mathbf{0} \\ \mathbf{0} & \mathbf{0} & \mathbf{1}_2 & \mathbf{0} & \mathbf{0} & \mathbf{N}_\sigma^s \end{bmatrix} \\ \mathbf{N}_\sigma^m &= \mathbf{N}_\sigma^b = \mathbf{T}_\sigma^0 \begin{bmatrix} \eta - \bar{\eta} & 0 \\ 0 & \xi - \bar{\xi} \\ 0 & 0 \end{bmatrix} & \mathbf{N}_\sigma^s &= \tilde{\mathbf{T}}_\sigma^0 \begin{bmatrix} \eta - \bar{\eta} & 0 \\ 0 & \xi - \bar{\xi} \end{bmatrix} \end{aligned} \tag{18}$$

where the matrices

$$\mathbf{T}_\sigma^0 = \begin{bmatrix} J_{11}^0 J_{11}^0 & J_{21}^0 J_{21}^0 & 2J_{11}^0 J_{21}^0 \\ J_{12}^0 J_{12}^0 & J_{22}^0 J_{22}^0 & 2J_{12}^0 J_{22}^0 \\ J_{11}^0 J_{12}^0 & J_{21}^0 J_{22}^0 & J_{11}^0 J_{22}^0 + J_{12}^0 J_{21}^0 \end{bmatrix} \qquad \tilde{\mathbf{T}}_\sigma^0 = \begin{bmatrix} J_{11}^0 & J_{21}^0 \\ J_{12}^0 & J_{22}^0 \end{bmatrix} \tag{19}$$

describe the transformation of contravariant tensor components to the local cartesian coordinate system at the element center. The constants $J^0_{\alpha\beta} = J_{\alpha\beta}(\xi = 0, \eta = 0)$ are the components of the Jacobian matrix $\mathbf{J}$ in eq. (10) evaluated at the element center.
The vector $\hat{\boldsymbol{\sigma}} \in \mathbb{R}^{14}$ contains 8 parameters for the constant part and 6 parameters for the varying part of the stress field, respectively. The interpolation of the membrane forces and bending moments corresponds to the procedure in Ref. [19], see also the original approach for plane stress problems with $\bar{\xi} = \bar{\eta} = 0$ in Ref. [20]. Due to the constants

$$\bar{\xi} = \frac{1}{A_e} \int\limits_{(\Omega_e)} \xi \, dA \qquad \bar{\eta} = \frac{1}{A_e} \int\limits_{(\Omega_e)} \eta \, dA \qquad A_e = \int\limits_{(\Omega_e)} dA \tag{20}$$

the linear functions are orthogonal to the constant function which yields partly decoupled matrices. The area element $dA = j \, d\xi d\eta$ is given with $j(\xi, \eta) = |\mathbf{X}^h_{,\xi} \times \mathbf{X}^h_{,\eta}|$. Concerning stability of the discrete system of equations we refer to the discussion in Ref. [16].

3.3 Interpolation of the shell strains

The interpolation of the independent shell strains consists of two parts. The first part with 14 parameters corresponds to the last section, whereas the second part with 2 to 12 parameters corresponds to the enhanced strain interpolation introduced in Ref. [9]. The functions of the second part are chosen orthogonal to the stress interpolation. In this context we also refer to References [21, 22, 23], where mixed-enhanced strain methods have been investigated. Thus we have

$$\boldsymbol{\varepsilon}^h = [\mathbf{N}^1_\varepsilon, \mathbf{N}^2_\varepsilon] \begin{bmatrix} \hat{\boldsymbol{\varepsilon}}_1 \\ \hat{\boldsymbol{\varepsilon}}_2 \end{bmatrix} = \mathbf{N}_\varepsilon \, \hat{\boldsymbol{\varepsilon}} \qquad \hat{\boldsymbol{\varepsilon}}_1 \in \mathbb{R}^{14} \,, \; \hat{\boldsymbol{\varepsilon}}_2 \in \mathbb{R}^\beta \quad \beta = 2, 4, 6, 8, 10, 12$$

$$\mathbf{N}^1_\varepsilon = \begin{bmatrix} \mathbf{1}_3 & \mathbf{0} & \mathbf{0} & \mathbf{N}^{m1}_\varepsilon & \mathbf{0} & \mathbf{0} \\ \mathbf{0} & \mathbf{1}_3 & \mathbf{0} & \mathbf{0} & \mathbf{N}^{b1}_\varepsilon & \mathbf{0} \\ \mathbf{0} & \mathbf{0} & \mathbf{1}_2 & \mathbf{0} & \mathbf{0} & \mathbf{N}^{s1}_\varepsilon \end{bmatrix} \,, \quad \mathbf{N}^2_\varepsilon = \begin{bmatrix} \mathbf{N}^{m2}_\varepsilon & \mathbf{0} & \mathbf{0} \\ \mathbf{0} & \mathbf{N}^{b2}_\varepsilon & \mathbf{0} \\ \mathbf{0} & \mathbf{0} & \mathbf{N}^{s2} \end{bmatrix}$$

$$\mathbf{N}^{m1}_\varepsilon = \mathbf{N}^{b1}_\varepsilon = \mathbf{T}^0_\varepsilon \begin{bmatrix} \eta - \bar{\eta} & 0 \\ 0 & \xi - \bar{\xi} \\ 0 & 0 \end{bmatrix} \,, \qquad \mathbf{N}^{m2}_\varepsilon = \mathbf{N}^{b2}_\varepsilon = \frac{j_0}{j} \left(\mathbf{T}^0_\sigma\right)^{-T} \mathbf{M}_\alpha \,, \alpha = 2, 4 \tag{21}$$

$$\mathbf{N}^{s1}_\varepsilon = \mathbf{N}^s_\sigma \,, \qquad \mathbf{N}^{s2}_\varepsilon = \frac{j_0}{j} \left(\tilde{\mathbf{T}}^0_\sigma\right)^{-T} \tilde{\mathbf{M}}_\alpha \,, \alpha = 2, 4$$

with $j_0 = j \, (\xi = 0, \eta = 0)$ and

$$\mathbf{T}^0_\varepsilon = \begin{bmatrix} J^0_{11} J^0_{11} & J^0_{21} J^0_{21} & J^0_{11} J^0_{21} \\ J^0_{12} J^0_{12} & J^0_{22} J^0_{22} & J^0_{12} J^0_{22} \\ 2 J^0_{11} J^0_{12} & 2 J^0_{21} J^0_{22} & J^0_{11} J^0_{22} + J^0_{12} J^0_{21} \end{bmatrix} . \tag{22}$$

$$\mathbf{M}_2 = \begin{bmatrix} \tilde{\mathbf{M}}_2 \\ \mathbf{0}_{1\times 2} \end{bmatrix} \,, \; \mathbf{M}_4 = \begin{bmatrix} \tilde{\mathbf{M}}_4 \\ \mathbf{0}_{1\times 4} \end{bmatrix} \,, \quad \tilde{\mathbf{M}}_2 = \begin{bmatrix} \xi & 0 \\ 0 & \eta \end{bmatrix} \,, \; \tilde{\mathbf{M}}_4 = \begin{bmatrix} \xi & 0 & \xi\eta & 0 \\ 0 & \eta & 0 & \xi\eta \end{bmatrix} \tag{23}$$

3.4 Linearized variational formulation

Assuming conservative external loads $\bar{\mathbf{p}}$ and $\bar{\mathbf{t}}$ the linearization of the stationary condition (5) reads

$$
\begin{aligned}
&L\,[g(\boldsymbol{\theta},\delta\boldsymbol{\theta}),\Delta\boldsymbol{\theta}] := g(\boldsymbol{\theta},\delta\boldsymbol{\theta}) + Dg\cdot\Delta\boldsymbol{\theta} \\
&Dg\cdot\Delta\boldsymbol{\theta} = \int_{(\Omega)} [\delta\boldsymbol{\varepsilon}^T(\mathbf{C}\,\Delta\boldsymbol{\varepsilon}-\Delta\boldsymbol{\sigma}) + \delta\boldsymbol{\sigma}^T(\Delta\boldsymbol{\varepsilon}_G-\Delta\boldsymbol{\varepsilon}) + \delta\boldsymbol{\varepsilon}_G^T\Delta\boldsymbol{\sigma} + \Delta\delta\boldsymbol{\varepsilon}_G^T\boldsymbol{\sigma}]\,dA\,.
\end{aligned}
\tag{24}
$$

with $\mathbf{C} = \partial^2_{\boldsymbol{\varepsilon}} W$. Hence inserting above interpolations for the displacements, stresses and strains yields the finite element approximation

$$
L\,[g(\boldsymbol{\theta}^h,\delta\boldsymbol{\theta}^h),\Delta\boldsymbol{\theta}^h] = \sum_{e=1}^{numel}
\begin{bmatrix} \delta\mathbf{v} \\ \delta\hat{\boldsymbol{\varepsilon}} \\ \delta\hat{\boldsymbol{\sigma}} \end{bmatrix}_e^T
\left\{
\begin{bmatrix} \mathbf{k}_g & \mathbf{0} & \mathbf{G}^T \\ \mathbf{0} & \mathbf{H} & -\mathbf{F} \\ \mathbf{G} & -\mathbf{F}^T & \mathbf{0} \end{bmatrix}
\begin{bmatrix} \Delta\mathbf{v} \\ \Delta\hat{\boldsymbol{\varepsilon}} \\ \Delta\hat{\boldsymbol{\sigma}} \end{bmatrix}
+
\begin{bmatrix} \mathbf{f}^i - \mathbf{f}^a \\ \mathbf{f}^e \\ \mathbf{f}^s \end{bmatrix}
\right\}_e
\tag{25}
$$

where *numel* denotes the total number of finite shell elements to discretize the problem. The following element matrices are defined

$$
\begin{aligned}
\mathbf{k}_g &= \int_{(\Omega_e)} \mathbf{k}_\sigma\,dA & \qquad \mathbf{f}^i &= \int_{(\Omega_e)} \mathbf{B}^T\boldsymbol{\sigma}^h\,dA = \mathbf{G}^T\,\hat{\boldsymbol{\sigma}} \\
\mathbf{H} &= \int_{(\Omega_e)} \mathbf{N}_\varepsilon^T\,\mathbf{C}\,\mathbf{N}_\varepsilon\,dA & \qquad \mathbf{f}^e &= \int_{(\Omega_e)} \mathbf{N}_\varepsilon^T\,(\partial_{\boldsymbol{\varepsilon}} W - \boldsymbol{\sigma}^h)\,dA \\
\mathbf{F} &= \int_{(\Omega_e)} \mathbf{N}_\varepsilon^T\,\mathbf{N}_\sigma\,dA & \qquad \mathbf{f}^s &= \int_{(\Omega_e)} \mathbf{N}_\sigma^T\,\boldsymbol{\varepsilon}_G^h\,dA - \mathbf{F}^T\,\hat{\boldsymbol{\varepsilon}} \\
\mathbf{G} &= \int_{(\Omega_e)} \mathbf{N}_\sigma^T\,\mathbf{B}\,dA\,,
\end{aligned}
\tag{26}
$$

with $\mathbf{B} = [\mathbf{B}_1,\mathbf{B}_2,\mathbf{B}_3,\mathbf{B}_4]$. Here $\mathbf{B}_I$ is derived in Appendix A and $\mathbf{k}_\sigma$ in Appendix B. Furthermore, the computation of the stress resultants $\partial_{\boldsymbol{\varepsilon}} W$ and material matrix $\mathbf{C}$ is explicitly described in Appendix C. The vector of the external loads $\mathbf{f}^a$ corresponds to the standard displacement formulation. The integrals in (20) and (26) are computed numerically using a 2×2 Gauss integration scheme. For the geometrical and physical linear case an analytical integration of all matrices is possible along with a flat projection, see Ref. [24] on basis of a Hellinger–Reissner functional.

We continue with $L[g(\boldsymbol{\theta}^h,\delta\boldsymbol{\theta}^h),\Delta\boldsymbol{\theta}^h] = 0$, where $\delta\boldsymbol{\theta}^h \neq \mathbf{0}$ and obtain

$$
\begin{aligned}
&\mathbf{k}_g\,\Delta\mathbf{v} + \mathbf{G}^T\,\Delta\hat{\boldsymbol{\sigma}} + \mathbf{f}^i - \mathbf{f}^a = \mathbf{r} \\
&\mathbf{H}\,\Delta\hat{\boldsymbol{\varepsilon}} - \mathbf{F}\,\Delta\hat{\boldsymbol{\sigma}} + \mathbf{f}^e = \mathbf{0} \\
&\mathbf{G}\,\Delta\mathbf{v} - \mathbf{F}^T\,\Delta\hat{\boldsymbol{\varepsilon}} + \mathbf{f}^s = \mathbf{0}\,,
\end{aligned}
\tag{27}
$$

where $\mathbf{r}$ denotes the vector of element nodal forces.

Since the stresses and strains are interpolated discontinuously across the element boundaries the parameters $\Delta\hat{\boldsymbol{\varepsilon}}$ and $\Delta\hat{\boldsymbol{\sigma}}$ can be eliminated from the last two equations

$$\begin{aligned} \Delta\hat{\boldsymbol{\varepsilon}} &= \mathbf{H}^{-1}\,(\mathbf{F}\,\Delta\hat{\boldsymbol{\sigma}} - \mathbf{f}^e) \\ \Delta\hat{\boldsymbol{\sigma}} &= \hat{\mathbf{H}}\,[\mathbf{G}\,\Delta\mathbf{v} + (\mathbf{f}^s + \mathbf{F}^T\mathbf{H}^{-1}\mathbf{f}^e)] \qquad\qquad \hat{\mathbf{H}} = (\mathbf{F}^T\,\mathbf{H}^{-1}\,\mathbf{F})^{-1}\,. \end{aligned} \tag{28}$$

Inserting (28) in $(27)_1$ yields the tangential element stiffness matrix $\mathbf{k}_T^e$ and the element residual vector $\hat{\mathbf{f}}$

$$\begin{aligned} L\,[g(\boldsymbol{\theta}^h, \delta\boldsymbol{\theta}^h), \Delta\boldsymbol{\theta}^h] &= \sum_{e=1}^{numel} \delta\mathbf{v}^T(\mathbf{k}_T^e\,\Delta\mathbf{v} + \hat{\mathbf{f}}) = 0 \\ \mathbf{k}_T^e &= \mathbf{G}^T\,\hat{\mathbf{H}}\,\mathbf{G} + \mathbf{k}_g \\ \hat{\mathbf{f}} &= \mathbf{G}^T\,[\hat{\boldsymbol{\sigma}} + \hat{\mathbf{H}}\,(\mathbf{f}^s + \mathbf{F}^T\,\mathbf{H}^{-1}\,\mathbf{f}^e)] - \mathbf{f}^a \end{aligned} \tag{29}$$

The explicit computation of $\mathbf{H}^{-1}$ is not necessary. Concerning an effective elimination of the stress and strain parameters on the element level we refer to Appendix D. The linear element matrix possesses with six zero eigenvalues the correct rank.
The global matrices are obtained by standard assembly procedures

$$\mathbf{K}_T = \mathop{\mathsf{A}}_{e=1}^{numel} \mathbf{k}_T^e \qquad\qquad \hat{\mathbf{F}} = \mathop{\mathsf{A}}_{e=1}^{numel} \hat{\mathbf{f}}\,. \tag{30}$$

where A denotes the assembly operator. The solution of the global system of equations yields the increment of the global displacement vector $\Delta\mathbf{V} = -\mathbf{K}_T^{-1}\,\hat{\mathbf{F}}$ and thus the increments $\Delta\mathbf{u}_K$ and $\Delta\boldsymbol{\beta}_K$ at each node. Here, one has to consider transformation

$$\Delta\boldsymbol{\omega}_K = \mathbf{T}_{3K}\,\Delta\boldsymbol{\beta}_K \qquad \mathbf{T}_{3K} = \begin{cases} \mathbf{1}_3 & \text{for nodes on shell intersections} \\ [\mathbf{a}_{1K}, \mathbf{a}_{2K}]_{(3\times 2)} & \text{for all other nodes} \end{cases} \tag{31}$$

which is discussed in Appendix A. Thus the element possesses six degrees of freedom at nodes on intersections and five at all other nodes. In this context we also refer to References [25, 26]. The update of the nodal displacements is performed in a standard way on the system level,

$$\begin{aligned} \mathbf{u}_K &\Longleftarrow \mathbf{u}_K + \Delta\mathbf{u}_K \\ \boldsymbol{\omega}_K &\Longleftarrow \boldsymbol{\omega}_K + \Delta\boldsymbol{\omega}_K \end{aligned} \qquad \hat{\boldsymbol{\sigma}} \Longleftarrow \hat{\boldsymbol{\sigma}} + \Delta\hat{\boldsymbol{\sigma}} \qquad \hat{\boldsymbol{\varepsilon}} \Longleftarrow \hat{\boldsymbol{\varepsilon}} + \Delta\hat{\boldsymbol{\varepsilon}}\,, \tag{32}$$

whereas the stress and strain parameters are updated on the element level using (28). For this purpose the matrices which are necessary for the update have to be stored for each element. For linear elasticity with $\mathbf{C}$ = constant follows $\mathbf{H}$ = constant. Considering $(28)_1$ one can see that $\mathbf{f}^e = \mathbf{0}$ holds for the equilibrium state. Thus with (26)

$$\mathbf{f}^e = \mathbf{H}\,\hat{\boldsymbol{\varepsilon}} - \mathbf{F}\hat{\boldsymbol{\sigma}} \equiv \mathbf{0} \tag{33}$$

holds for the whole iteration process.

4 Examples

The derived element formulation has been implemented in an extended version of the general purpose finite element program FEAP, see Zienkiewicz and Taylor, Ref. [27].

4.1 Membrane and bending patch test

First we investigate the element behaviour within a constant membrane and bending patch test as is depicted in Fig. 2, see also Ref. [28]. A rectangular plate of length a and width b is supported at three corners. We consider in–plane loading and bending loading denoted by load case 1 and 2, respectively. Both, membrane and bending patch test are fulfilled by the present element with constant normal forces $n_x = 1, n_y = n_{xy} = 0$ (load case 1) and constant bending moments $m_x = m_y = m_{xy} = 1$ (load case 2).

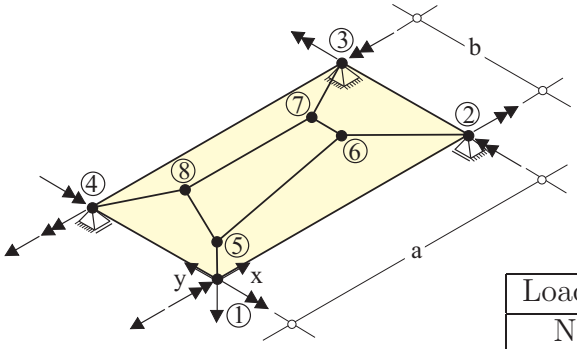

$a = 40$ $\quad E = 10^6$
$b = 20$ $\quad \nu = 0.3$
$h = 0.1$

Load case	1	2		
Node	F_x	F_z	$\bar{m}_x$	$\bar{m}_y$
1	-20	-2	20	-10
2	0	0	20	10
3	0	0	-20	10
4	-20	0	-20	-10

Figure 2: Rectangular plate, patch of 5 elements

4.2 Annular plate

This example, which is shown in Figure 3, has been introduced in Ref. [29]. The annular plate is loaded at its free edge with a load $\lambda \cdot \bar{p}$; the other edge is clamped. Here, λ denotes the load factor and $\bar{p} = 0.1$ a constant load. The geometrical and material data are:

$$\begin{aligned} E_1 &= 40 \cdot 10^6 & R_1 &= 6 \\ E_2 &= 1 \cdot 10^6 & R_2 &= 10 \\ G_{12} = G_{23} &= 0.6 \cdot 10^6 & h &= 0.04 \\ \nu_{12} &= 0.25 & h_1 = h_2 = h_3 &= h/3 \end{aligned}$$

The analysis is based on a 6×30 mesh for the stacking sequences $[0°, 90°, 0°]$, $[90°, 0°, 90°]$ and $[45°, -45°, 45°]$. Here, $0°$ and $90°$ means circumferential direction and radial direction, respectively. Here, 4/4/0 denotes the number of interpolation parameters for membrane, bending and shear, see Eq. (21). The results are plotted in Figs. 4 - 5 for the respective layer sequences. As can be seen there is good agreement with the displacement model, Ref. [30]. For the $[45°, -45°, 45°]$ stacking sequence the present element shows a weaker behaviour. Adding the interpolation functions of the second part leads to further improvements. In Tab. 1 a convergence study is presented for the displacements u_A and u_B at a load level $\lambda = 1$. This example shows clearly the better convergence behaviour of the element itself and the superior behaviour of the refined strain interpolation. It is emphasized that for the considered

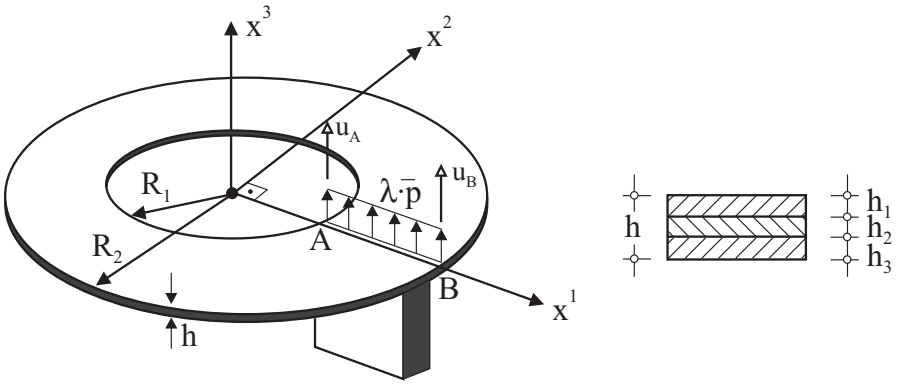

Figure 3: Annular plate

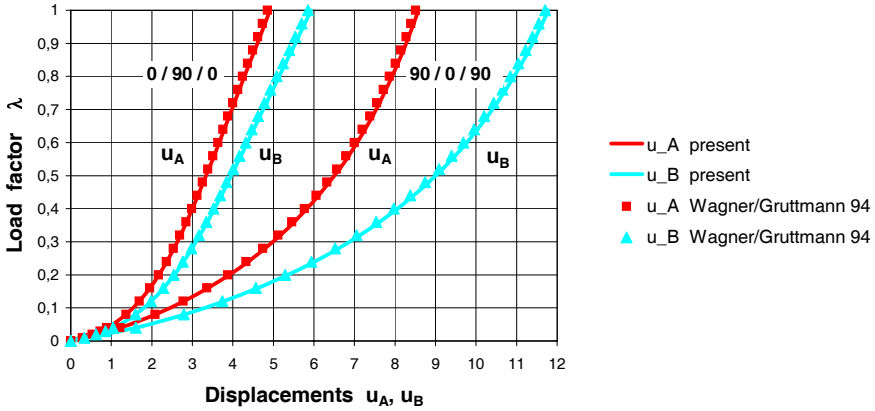

Figure 4: Load displacement curves for $[0°, 90°, 0°]$ and $[90°, 0°, 90°]$ stacking sequences

layer sequence coupling between membrane and bending occurs. The numerical investigations show, that the use of two additional parameters for membrane as well as bending terms are sufficient. Four parameters together with the matrix $\mathbf{M}_4$ as well as the application of the concept to the transverse shear strains lead not to a significant improvement of the element behaviour.

For the $[0°, 90°, 0°]$ stacking sequence the load can be applied within one single load step, see Tab. 2 in case of a 6×30-mesh, whereas the displacement model, Ref. [30], requires 4 load steps to calculate the final configuration. Similar results hold for the other stacking sequences. The superior iteration behaviour is shown also in Tab. 3 for two load steps of the same problem. The present formulation needs only about one third of the number of iterations. This demonstrates clearly the robustness of the new developed mixed hybrid element. Finally Fig. 6 shows a plot of the deformed configuration.

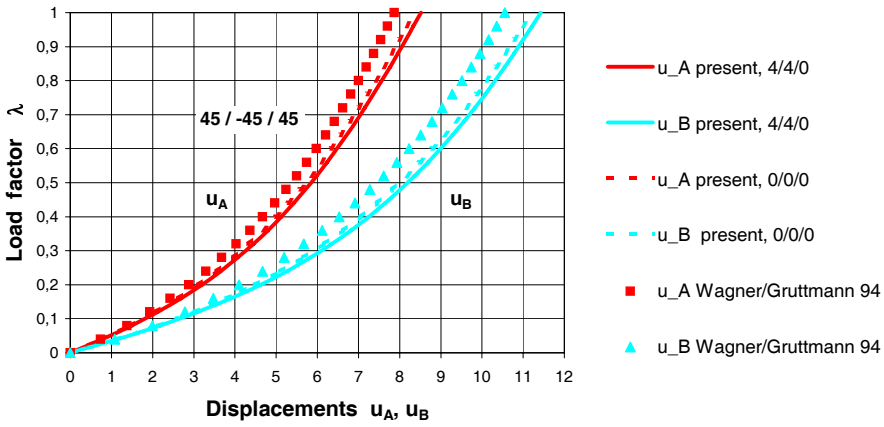

Figure 5: Load displacement curves for $[45°, -45°, 45°]$ stacking sequence

Table 1: Displacements u_A und u_B at load level $\lambda = 1$ for different elements and meshes and a $[45°, -45°, 45°]$ stacking sequence

Mesh	Ref. [30]		Present									
			0/0/0		2/0/0		0/2/0		2/2/0		2/2/2	
	u_A	u_B	u_A	u_B	u_A	u_B	u_A	u_B	u_A	u_B	u_A	u_B
1×8	5.82	8.44	7.03	10.17	7.52	10.72	7.81	10.95	8.14	11.39	8.14	11.39
3×15	6.46	8.83	7.91	10.68	8.20	11.11	8.10	10.87	8.40	11.31	8.40	11.31
6×30	7.87	10.55	8.35	11.20	8.46	11.37	8.40	11.26	8.52	11.43	8.52	11.43
12×60	8.35	11.16	8.50	11.39	8.53	11.44	8.51	11.40	8.55	11.46	8.55	11.46
24×120	8.52	11.40	8.55	11.46	8.56	11.47	8.56	11.46	8.56	11.47	8.56	11.47

Mesh	Present											
	4/0/0		0/4/0		4/2/0		2/4/0		4/4/2		4/4/4	
	u_A	u_B	u_A	u_B	u_A	u_B	u_A	u_B	u_A	u_B	u_A	u_B
1×8	7.54	10.74	7.83	10.96	8.16	11.41	8.15	11.40	8.17	11.42	8.17	11.42
3×15	8.20	11.11	8.10	10.87	8.40	11.31	8.40	11.31	8.40	11.31	8.40	11.31
6×30	8.46	11.37	8.40	11.26	8.52	11.43	8.52	11.43	8.52	11.43	8.52	11.43
12×60	8.53	11.44	8.51	11.40	8.55	11.46	8.55	11.46	8.55	11.46	8.55	11.46
24×120	8.56	11.47	8.56	11.47	8.56	11.47	8.56	11.47	8.56	11.47	8.56	11.47

Table 2: Iteration of residual of present element for one single load step $\Delta\lambda = 1$, $[0°, 90°, 0°]$ stacking sequence and 6×30-mesh

No. of Iteration	Residual
1	$1.5634719E-01$
2	$3.9275413E+06$
3	$9.3384687E+05$
4	$9.4213733E+04$
5	$3.3242161E+04$
6	$4.9264341E+02$
7	$4.7236750E+02$
8	$1.5163524E+00$
9	$3.6369628E-05$
10	$6.2602028E-09$

Table 3: Iteration of residual for different elements for two load steps, $[0°, 90°, 0°]$ stacking sequence and 6×30-mesh

No. of Iteration	Step1 $\lambda = 0 \rightarrow \lambda = 0.1$		Step2 $\lambda = 0.1 \rightarrow \lambda = 0.5$	
	Ref. [30]	present	Ref. [30]	present
1	$1.5634719E-02$	$1.5634719E-02$	$6.2538877E-02$	$6.2538877E-02$
2	$2.6020011E+04$	$2.5746859E+04$	$2.8926444E+04$	$2.9767495E+04$
3	$6.5793165E+02$	$4.9387080E+03$	$9.4757811E+02$	$2.8315083E+03$
4	$3.3721291E+02$	$1.1463284E+02$	$9.6921690E+03$	$1.6466046E+02$
5	$2.7141014E+02$	$1.4038872E+00$	$8.3131313E+02$	$9.7474188E-02$
6	$2.2423866E+02$	$3.3273954E-04$	$2.9796023E+03$	$3.5539688E-08$
7	$2.2580338E+01$	$7.4140298E-09$	$1.9342202E+02$	
8	$4.6324640E+02$		$2.4089526E+03$	
9	$2.2074665E+00$		$3.5820831E+01$	
10	$1.2513383E+03$		$7.4108309E+02$	
11	$6.0837124E-01$		$2.6058553E+00$	
12	$2.1726471E+02$		$2.0458148E+03$	
13	$2.2742620E-02$		$1.5187721E+00$	
14	$1.8081783E+02$		$1.0776742E+02$	
15	$1.4264002E-02$		$4.3457229E-02$	
16	$7.3421111E-01$		$1.8600614E+02$	
17	$9.0950213E-05$		$1.4454398E-02$	
18	$1.0599305E-04$		$4.6287252E-01$	
19	$6.7454164E-09$		$3.1868428E-05$	
20			$6.3065865E-06$	
21			$5.9716093E-09$	

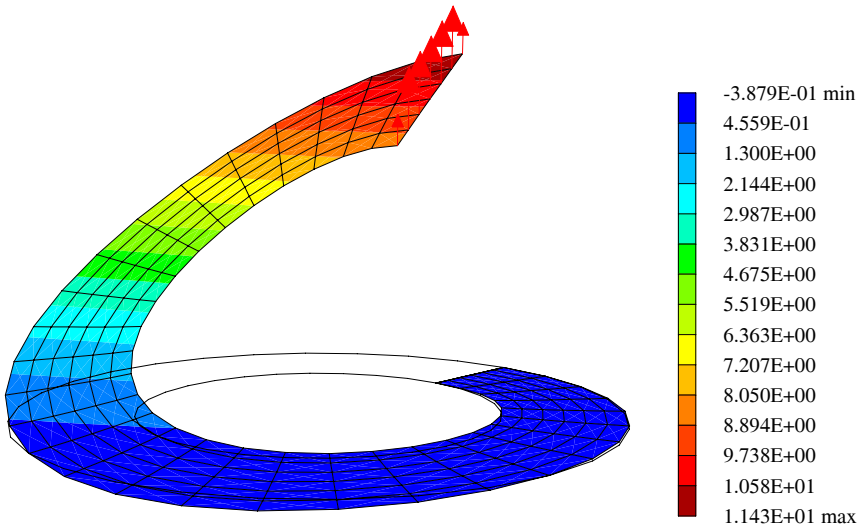

Figure 6: Vertical displacement and deformed mesh at load factor $\lambda = 1$ for the $[45°, -45°, 45°]$ stacking sequence and a 6×30-mesh

4.3 Hyperboloidal shell under two pairs of opposite loads

This problem was defined in Ref. [29], see also Ref. [30]. The hyperboloidal shell is loaded by two pairs of opposite loads. Considering symmetry only one eighth of the shell is discretized with a 16×16 element mesh, see Fig. 7. The shell is analyzed for two sets of laminate schemes. Both are of cross ply type with $[0°, 90°, 0°]$ and $[90°, 0°, 90°]$ stacking sequences, where $0°$ describes a fiber orientation in circumferential direction and $90°$ in meridian direction. The radius of the hyperboloidal shell is described by $R(x_3) = \frac{R_1}{c}\sqrt{c^2 + (x_3)^2}$ with $c = \frac{20}{\sqrt{3}}$ and the load is $P = 5$. The geometrical and material parameters are

$$\begin{array}{rclrcl} E_1 & = & 40 \cdot 10^6 & R_1 & = & 7.5 \\ E_2 & = & 1 \cdot 10^6 & R_2 & = & 15.0 \\ G_{12} = G_{23} & = & 0.6 \cdot 10^6 & H & = & 20.0 \\ \nu_{12} & = & 0.25 & h & = & 0.04 \end{array}$$

We compute the displacements of the depicted points A,B,C and D of the shell midsurface. The load deflection curves are plotted in Figures 8 to 11. As can be seen there is a good agreement with the results obtained with the shell model developed in Ref. [30]. The essential advantage of the present model is the robustness in the nonlinear equilibrium iterations. In Figs. 10 and 11 marks on the curves describe the maximal possible load steps for the respective element formulation. As the diagrams show the present element allows much larger load steps in comparison to the displacement model. The deformed configurations for a load factor $\lambda = 30$ in Fig. 12 are characterized by large displacements and finite rotations.

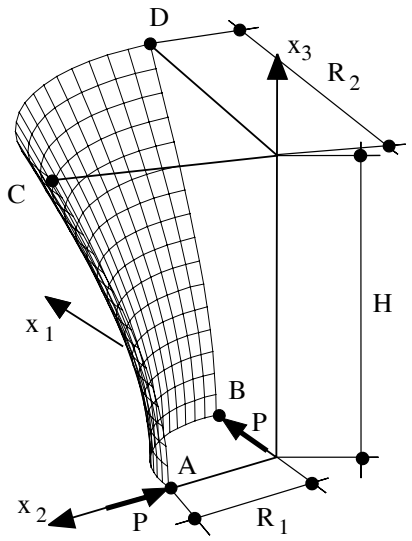

Figure 7: Hyperboloidal composite shell

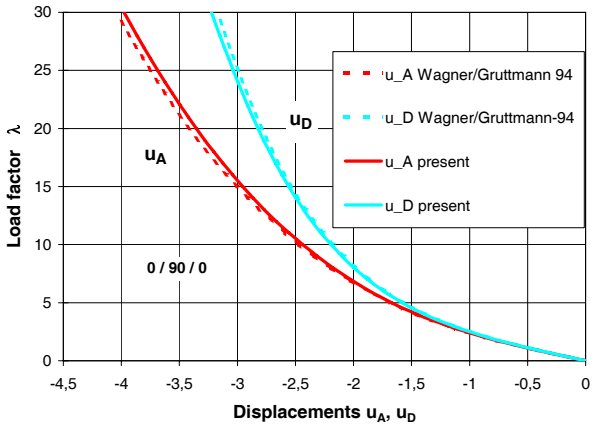

Figure 8: Hyperboloidal composite shell $[0°, 90°, 0°]$, $\lambda - u_A\,, \lambda - u_D$

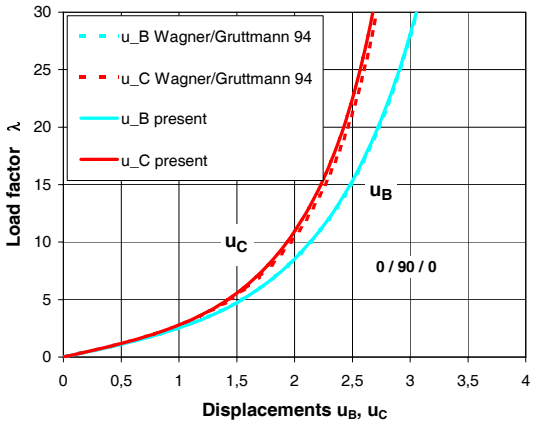

Figure 9: Hyperboloidal composite shell $[0°, 90°, 0°]$, $\lambda - u_B\,, \lambda - u_C$

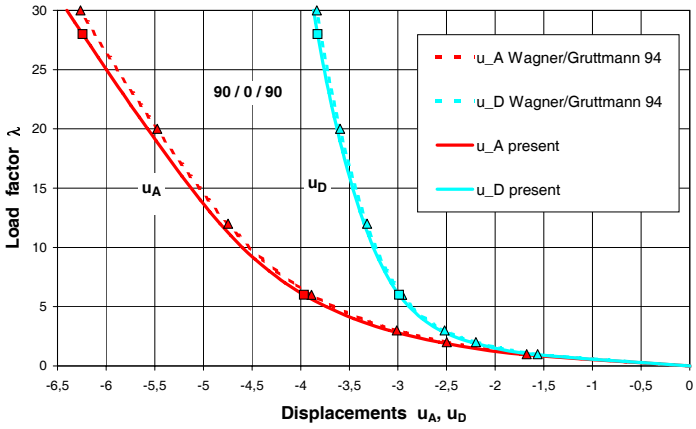

Figure 10: Hyperboloidal composite shell $[90°, 0°, 90°]$, $\lambda - u_A\,, \lambda - u_D$

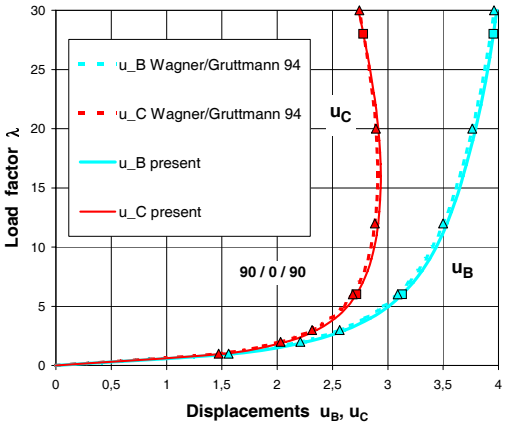

Figure 11: Hyperboloidal composite shell $[90°, 0°, 90°]$, $\lambda - u_B$, $\lambda - u_C$

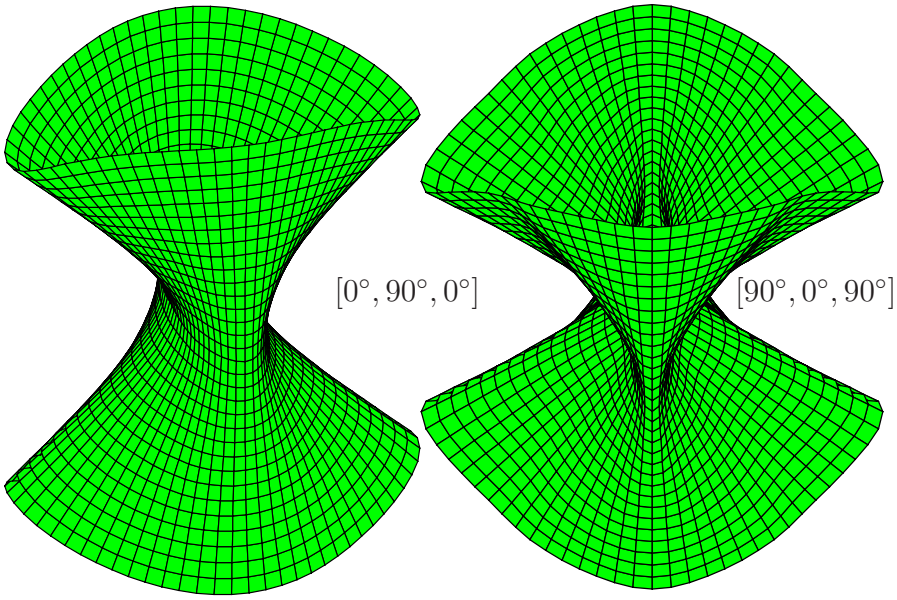

Figure 12: Hyperboloidal composite shell, deformed configurations for both laminates

4.4 Stability analysis of a stiffened cylindrical panel

With the last example we test the applicability of the present element to a more complicated industrial problem. The composite cylindrical panel, see Fig. 13, named PSC5 was produced by Israel Aircraft Industries (IAI) and tested by Abramovich, Weller et.al., see References [34, 35][1].

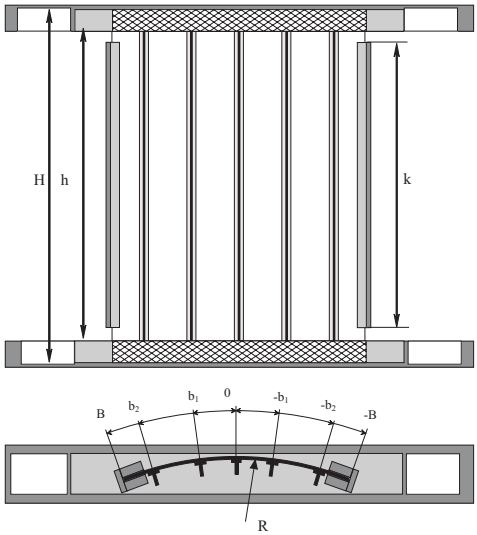

Dimensions of the panel in mm		Nominal Values
Skin middle surface radius	R	938
Arc-length of the panel	2B	680
Overall length of the panel	H	720
Skin thickness	s	1.0
Ply thickness	t	0.125
Number of stringers		5
Stringer distance	b1-0,b2-b1	136
Free edge distance	B-b2	68
Free length of panel	h	660
Length of the lateral edge supports	k	640

Figure 13: Composite panel PSC5 of IAI

In the test performed the uppermost and lowermost 30 mm of the panel was inside a frame filled with gypsum. The vertical edges of the panel was supported by a sliding support to keep the edges straight and preventing radial motion at the edges. Vertical displacement was controlled by the testing-machine at the upper edge of the stiffened panel, while the lower edge of the panel was fixed. The axial load was thus introduced directly into both the skin and the stiffeners.
The chosen finite element mesh consist of 72 elements in the longitudinal direction, 50 in

[1] ©IAI Tel Aviv and Technion, I.I.T., Haifa, Israel

the circumferential direction and two elements in the height direction of the stringer blades giving a total of 4320 elements and 4453 nodes. The elements are positioned in the middle surface of the skin and the stringer blades. The eccentric position of the stringer foot is taken into account. This is possible with the present shell formulation since it allows consideration of an arbitrary reference surface. In the model the boundary conditions are applied to the nodes being 30 mm or less from the upper or lower edges of the panel and to the nodes at the vertical edges on the left and right side of the panel. In the skin all nodes being 30 mm or less from the upper or lower edges are prevented from radial motion. Nodes in the skin, at the skin-stiffener junction being 30 mm or less from the upper or lower panel edges, are also prevented from motion in the circumferential direction. The nodes at the vertical edges on the left and right side being more than 30 mm from the upper or lower edges of the panel are prevented from radial displacement. Vertical displacement was prescribed at the upper edge, while vertical displacement was prevented at the lower edge. The composite material is assumed to be linear elastic transversal isotropic with the following nominal values.

$$\begin{array}{rclrrcl} E_1 & = & 147300 \;\; MPa & \qquad & G_{12} & = & 6000 \;\; MPa \\ E_2 & = & 11800 \;\; MPa & & G_{23} & = & 3770 \;\; MPa \\ \nu_{12} & = & 0.3 & & & & \end{array}$$

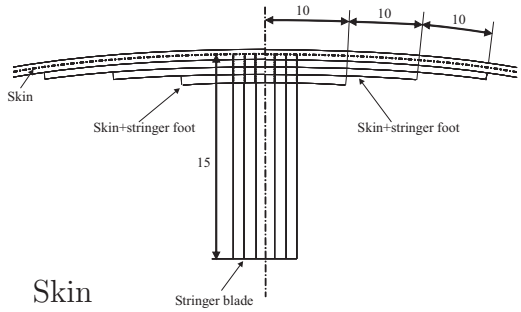

Skin
$[90°/45°/-45°/0°]_S$

Skin and stringer foot
$[90°/45°/-45°/0°]_S + (1-3) \times [90°/90°/-45°/45°]$

Stringer blade
$[45°/-45°/90°/90°]_{3S}$

Figure 14: Stacking sequences, position and dimensions of stringers of panel PSC5

The position and the dimensions of the stringers as well as the stacking sequences for the skin, the 3 gradations of the stringer foot and the stringer blade are defined in Fig. 14. Here, 0° describes a fiber orientation in circumferential direction and 90° in vertical direction. The +45°-direction is defined in an inside view of the panel in mathematical positive sense.
From the experiment it is known that the buckling behaviour of the panel is characterized by a nearly linear prebuckling behaviour, which is followed by a local skin buckling and an adjacent global buckling behaviour with two or more global buckles until collapse. A first static analysis has been performed using an arc–length–scheme together with accompanying actions like e.g. inspection of the determinant, see e.g. Ref. [36]. Results could only be achieved until the first buckling load at the end of the prebuckling region. Here, a cluster of zero eigenvalues associated with local buckling patterns occurs at nearly the same load,

which leads always to divergence in the equilibrium iterations. Two methods are available to overcome these problems. Either one can add artificial damping forces or one can choose a transient quasistatic analysis, which has been done here. The extension of the finite element formulation for dynamical loads is a standard procedure. The variation of the Lagrange function $L = T - V$ must be zero within the time range

$$\delta I = \delta \int_0^T L \, dt = 0 \,. \tag{34}$$

Here, T is the total kinetic energy of the shell, which consists of the translatoric part of the reference surface and the rotatoric part of the un-extensible director vector. The total potential energy V corresponds to Eq. (1). After variation and adjacent partial integration with respect to the time it follows the variational form including the inertia terms. Introducing the shape functions for displacements, stresses and strains and the assembly procedure, one ends up with a system of equations for the unknown discrete displacements, velocities and accelerations. Out of the field of time integration schemes we choose the well known HHT–algorithm, Ref. [37], with $\alpha = 0.05$, where numerical damping is included. A total prescribed displacement of $u = 3$ mm is calculated in 500 equal time steps of 0.012 sec. with $\rho = 1.6 \cdot 10^{-6}$N sec^2/mm^4. The total axial load P with respect to the prescribed axial displacement

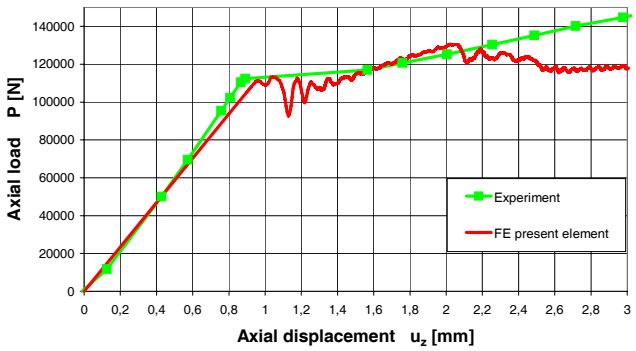

Figure 15: Axial load – axial deflection u_z of panel PSC5

u_z of the top of the panel is depicted in Fig. 15. The curve is characterized by a nearly linear prebuckling behaviour, see Fig. 16_1. Due to the panel design skin buckling occurs before global buckling, see Figs.16_2. A good agreement between experiment and the numerical modeling of the associated load can be seen. The further deformation pattern is governed by two global buckles, see Fig.16_{2-4}, which changes dynamically to three buckles, see Fig.16_{5+6}, within the calculated range.

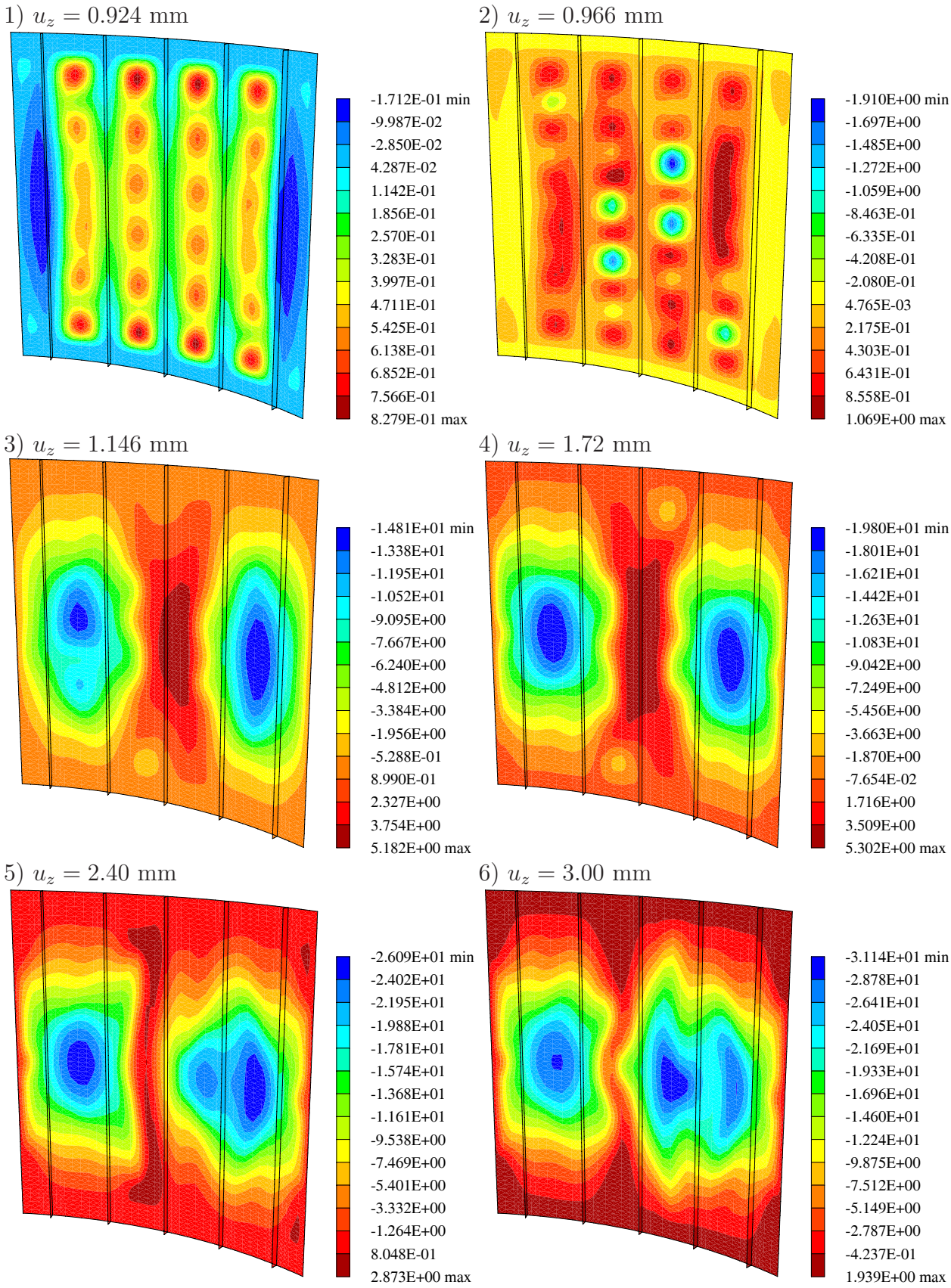

Figure 16: Radial displacements at vertical displacements $u_z = 0.924, 0.966, 1.146, 1.72, 2.4$ and 3.00 mm

5 Conclusions

The paper deals with the structural analysis of laminated shells using a mixed hybrid shell element. Using a three field variational principle appropriate interpolation functions for the independent mechanical fields are described. The approximation of the shell strains is improved introducing additional interpolation functions. The numerical tests show that two parameters for membrane as well as for bending terms are sufficient for the second interpolation part. The element performance has been illustrated by several numerical examples which include bifurcation and post–buckling response. Especially for large rigid body motions the new formulation allows very large load steps and requires essentially less equilibrium iterations in comparison to displacement based elements.

Acknowledgements
A part of this work of the second author is supported by the European Commission, Priority Aeronautics and Space, Contract AST3-CT-2003-502723 which is gratefully appreciated. The associated information in this paper is provided as is and no guarantee or warranty is given that the information is fit for any particular purpose. The user thereof uses the information at its sole risk and liability.

Appendix

A First variation of the shell strains

The first variation of the shell strains is derived from (15) and (16)

$$\delta\boldsymbol{\varepsilon}_G^h = \begin{bmatrix} \delta\varepsilon_{11}^h \\ \delta\varepsilon_{22}^h \\ 2\delta\varepsilon_{12}^h \\ \delta\kappa_{11}^h \\ \delta\kappa_{22}^h \\ 2\delta\kappa_{12}^h \\ \delta\gamma_1^h \\ \delta\gamma_2^h \end{bmatrix} = \begin{bmatrix} \delta\mathbf{x}_{,1}^h \cdot\mathbf{x}_{,1}^h \\ \delta\mathbf{x}_{,2}^h \cdot\mathbf{x}_{,2}^h \\ \delta\mathbf{x}_{,1}^h \cdot\mathbf{x}_{,2}^h + \delta\mathbf{x}_{,2}^h \cdot\mathbf{x}_{,1}^h \\ \delta\mathbf{x}_{,1}^h \cdot\mathbf{d}_{,1}^h + \delta\mathbf{d}_{,1}^h \cdot\mathbf{x}_{,1}^h \\ \delta\mathbf{x}_{,2}^h \cdot\mathbf{d}_{,2}^h + \delta\mathbf{d}_{,2}^h \cdot\mathbf{x}_{,2}^h \\ \delta\mathbf{x}_{,1}^h \cdot\mathbf{d}_{,2}^h + \delta\mathbf{x}_{,2}^h \cdot\mathbf{d}_{,1}^h + \delta\mathbf{d}_{,1}^h \cdot\mathbf{x}_{,2}^h + \delta\mathbf{d}_{,2}^h \cdot\mathbf{x}_{,1}^h \\ \mathbf{J}^{-1} \begin{Bmatrix} \frac{1}{2}[(1-\eta)\,\delta\gamma_\xi^B + (1+\eta)\,\delta\gamma_\xi^D \\ \frac{1}{2}[(1-\xi)\,\delta\gamma_\eta^A + (1+\xi)\,\delta\gamma_\eta^C] \end{Bmatrix} \end{bmatrix} \tag{35}$$

with

$$\begin{aligned} \delta\gamma_\xi^M &= [\delta\mathbf{x}_{,\xi}\cdot\mathbf{d} + \mathbf{x}_{,\xi}\cdot\delta\mathbf{d}]^M \qquad & M &= B, D \\ \delta\gamma_\eta^L &= [\delta\mathbf{x}_{,\eta}\cdot\mathbf{d} + \mathbf{x}_{,\eta}\cdot\delta\mathbf{d}]^L \qquad & L &= A, C\,, \end{aligned} \tag{36}$$

where $\delta\mathbf{x}_{,\xi}\,, \delta\mathbf{x}_{,\eta}\,, \delta\mathbf{d}$ are evaluated at the midside nodes considering (17).
The virtual vectors $\delta\mathbf{x}_{,\alpha}^h$ and $\delta\mathbf{d}_{,\alpha}^h$ using (13) are determined

$$\delta\mathbf{x}_{,\alpha}^h = \sum_{I=1}^{4} N_{I,\alpha}\;\delta\mathbf{u}_I \qquad\qquad \delta\mathbf{d}_{,\alpha}^h = \sum_{I=1}^{4} N_{I,\alpha}\;\delta\mathbf{d}_I\,, \tag{37}$$

with the virtual nodal displacements $\delta\mathbf{u}_I$ and

$$\delta\mathbf{d}_I = \delta\mathbf{w}_I \times \mathbf{d}_I = \mathbf{W}_I^T\,\delta\mathbf{w}_I \qquad\qquad \mathbf{W}_I = \operatorname{skew}\mathbf{d}_I \tag{38}$$

where according to Ref. [31]

$$\delta\mathbf{w}_I = \mathbf{H}_I\,\delta\boldsymbol{\omega}_I\,, \qquad\qquad \mathbf{H}_I = \mathbf{1} + \frac{1-\cos\omega_I}{\omega_I^2}\,\boldsymbol{\Omega}_I + \frac{\omega_I - \sin\omega_I}{\omega_I^3}\,\boldsymbol{\Omega}_I^2\,. \tag{39}$$

At nodes which are not positioned on intersections a drilling stiffness is not available and a transformation of the virtual rotation vector to the local coordinate system is necessary:

$$\begin{aligned} \delta\boldsymbol{\omega}_I = \mathbf{T}_{3I}\,\delta\boldsymbol{\beta}_I \quad \mathbf{T}_{3I} &= \begin{cases} \mathbf{1}_3 & \text{for nodes on shell intersections} \\ [\mathbf{a}_{1I}, \mathbf{a}_{2I}]_{(3\times 2)} & \text{for all other nodes} \end{cases} \\ \delta\boldsymbol{\beta}_I &= \begin{cases} [\delta\beta_{xI}, \delta\beta_{yI}, \delta\beta_{zI}]^T & \text{for nodes on shell intersections} \\ [\delta\beta_{1I}, \delta\beta_{2I}]^T & \text{for all other nodes} \end{cases} \end{aligned} \tag{40}$$

where $\delta\beta_{\alpha I}$ denote local rotations. Next combining (38) – (40) we obtain

$$\delta\mathbf{d}_I = \mathbf{T}_I\,\delta\boldsymbol{\beta}_I \qquad\qquad \mathbf{T}_I = \mathbf{W}_I^T\mathbf{H}_I\mathbf{T}_{3I} \tag{41}$$

Finally we are able to summarize the finite element approximation of the virtual shell strains (35) considering (36) - (41)

$$\begin{bmatrix} \delta\varepsilon^h_{11} \\ \delta\varepsilon^h_{22} \\ 2\delta\varepsilon^h_{12} \\ \delta\kappa^h_{11} \\ \delta\kappa^h_{22} \\ 2\delta\kappa^h_{12} \\ \delta\gamma^h_1 \\ \delta\gamma^h_2 \end{bmatrix} = \sum_{I=1}^{4} \begin{bmatrix} N_{I,1}\,\mathbf{x}^T_{,1} & \mathbf{0} \\ N_{I,2}\,\mathbf{x}^T_{,2} & \mathbf{0} \\ N_{I,1}\,\mathbf{x}^T_{,2} + N_{I,2}\,\mathbf{x}^T_{,1} & \mathbf{0} \\ N_{I,1}\,\mathbf{d}^T_{,1} & N_{I,1}\,\mathbf{b}^T_{I1} \\ N_{I,2}\,\mathbf{d}^T_{,2} & N_{I,2}\,\mathbf{b}^T_{I2} \\ N_{I,1}\,\mathbf{d}^T_{,2} + N_{I,2}\,\mathbf{d}^T_{,1} & N_{I,1}\,\mathbf{b}^T_{I2} + N_{I,2}\,\mathbf{b}^T_{I1} \\ \mathbf{J}^{-1} \begin{Bmatrix} N_{I,\xi}\,\mathbf{d}^T_M \\ N_{I,\eta}\,\mathbf{d}^T_L \end{Bmatrix} & \mathbf{J}^{-1} \begin{Bmatrix} N_{I,\xi}\,\xi_I\,\mathbf{b}^T_M \\ N_{I,\eta}\,\eta_I\,\mathbf{b}^T_L \end{Bmatrix} \end{bmatrix} \begin{bmatrix} \delta\mathbf{u}_I \\ \delta\boldsymbol{\beta}_I \end{bmatrix} \tag{42}$$

$$\delta\boldsymbol{\varepsilon}^h_G = \sum_{I=1}^{4} \mathbf{B}_I\,\delta\mathbf{v}_I$$

with $\mathbf{b}_{I\alpha} = \mathbf{T}^T_I\,\mathbf{x}_{,\alpha}$, $\mathbf{b}_M = \mathbf{T}^T_I\,\mathbf{x}^M_{,\xi}$ and $\mathbf{b}_L = \mathbf{T}^T_I\,\mathbf{x}^L_{,\eta}$. The allocation of the midside nodes to the corner nodes is given by

$$(I, M, L) \in \{(1, B, A); (2, B, C); (3, D, C); (4, D, A)\}\,. \tag{43}$$

B Second variation of the shell strains

The linearized virtual shell strains read

$$\Delta\delta\boldsymbol{\varepsilon}^h_G = \begin{bmatrix} \Delta\delta\varepsilon^h_{11} \\ \Delta\delta\varepsilon^h_{22} \\ 2\Delta\delta\varepsilon^h_{12} \\ \Delta\delta\kappa^h_{11} \\ \Delta\delta\kappa^h_{22} \\ 2\Delta\delta\kappa^h_{12} \\ \\ \Delta\delta\gamma^h_1 \\ \Delta\delta\gamma^h_2 \end{bmatrix} = \begin{bmatrix} \delta\mathbf{x}^h_{,1}\cdot\Delta\mathbf{x}^h_{,1} \\ \delta\mathbf{x}^h_{,2}\cdot\Delta\mathbf{x}^h_{,2} \\ \delta\mathbf{x}^h_{,1}\cdot\Delta\mathbf{x}^h_{,2} + \delta\mathbf{x}^h_{,2}\cdot\Delta\mathbf{x}^h_{,1} \\ \delta\mathbf{x}^h_{,1}\cdot\Delta\mathbf{d}^h_{,1} + \delta\mathbf{d}^h_{,1}\cdot\Delta\mathbf{x}^h_{,1} + \mathbf{x}^h_{,1}\cdot\Delta\delta\mathbf{d}^h_{,1} \\ \delta\mathbf{x}^h_{,2}\cdot\Delta\mathbf{d}^h_{,2} + \delta\mathbf{d}^h_{,2}\cdot\Delta\mathbf{x}^h_{,2} + \mathbf{x}^h_{,2}\cdot\Delta\delta\mathbf{d}^h_{,2} \\ \delta\mathbf{x}^h_{,1}\cdot\Delta\mathbf{d}^h_{,2} + \delta\mathbf{x}^h_{,2}\cdot\Delta\mathbf{d}^h_{,1} + \delta\mathbf{d}^h_{,1}\cdot\Delta\mathbf{x}^h_{,2} + \delta\mathbf{d}^h_{,2}\cdot\Delta\mathbf{x}^h_{,1} \\ \quad + \mathbf{x}^h_{,1}\cdot\Delta\delta\mathbf{d}^h_{,2} + \mathbf{x}^h_{,2}\cdot\Delta\delta\mathbf{d}^h_{,1} \\ \mathbf{J}^{-1} \begin{Bmatrix} \frac{1}{2}[(1-\eta)\,\Delta\delta\gamma^B_\xi + (1+\eta)\,\Delta\delta\gamma^D_\xi] \\ \frac{1}{2}[(1-\xi)\,\Delta\delta\gamma^A_\eta + (1+\xi)\,\Delta\delta\gamma^C_\eta] \end{Bmatrix} \end{bmatrix} \tag{44}$$

with

$$\begin{aligned} \Delta\delta\gamma^M_\xi &= [\delta\mathbf{x}_{,\xi}\cdot\Delta\mathbf{d} + \Delta\mathbf{x}_{,\xi}\cdot\delta\mathbf{d} + \mathbf{x}_{,\xi}\cdot\Delta\delta\mathbf{d}]^M \qquad M = B, D \\ \Delta\delta\gamma^L_\eta &= [\delta\mathbf{x}_{,\eta}\cdot\Delta\mathbf{d} + \Delta\mathbf{x}_{,\eta}\cdot\delta\mathbf{d} + \mathbf{x}_{,\eta}\cdot\Delta\delta\mathbf{d}]^L \qquad L = A, C \end{aligned} \tag{45}$$

The second variation of the current orthogonal base system has been derived in Ref. [31]

$$
\begin{aligned}
\mathbf{h}_I \cdot \Delta\delta\mathbf{d}_I &= \delta\mathbf{w}_I \cdot \mathbf{M}_I\, \Delta\mathbf{w}_I \\
\mathbf{M}_I(\mathbf{h}_I) &= \frac{1}{2}(\mathbf{d}_I \otimes \mathbf{h}_I + \mathbf{h}_I \otimes \mathbf{d}_I) + \frac{1}{2}(\mathbf{t}_I \otimes \boldsymbol{\omega}_I + \boldsymbol{\omega}_I \otimes \mathbf{t}_I) + c_{10}\mathbf{1} \\
\mathbf{t}_I &= -c_3\, \mathbf{b}_I + c_{11}\, (\mathbf{b}_I \cdot \boldsymbol{\omega}_I)\, \boldsymbol{\omega}_I \\
c_{10} &= \bar{c}_{10}\, (\mathbf{b}_I \cdot \boldsymbol{\omega}_I) - (\mathbf{d}_I \cdot \mathbf{h}_I) \\
\bar{c}_{10} &= \frac{\sin\omega_I - \omega_I}{2\omega_I\,(\cos\omega_I - 1)} \\
c_3 &= \frac{\omega_I\, \sin\omega_I + 2\,(\cos\omega_I - 1)}{\omega_I^2\,(\cos\omega_I - 1)} \\
c_{11} &= \frac{4\,(\cos\omega_I - 1) + \omega_I^2 + \omega_I \sin\omega_I}{2\,\omega_I^4\,(\cos\omega_I - 1)}
\end{aligned}
\tag{46}
$$

with an arbitrary vector $\mathbf{h}_I \in \mathbb{R}^3$ and $\mathbf{b}_I = \mathbf{d}_I \times \mathbf{h}_I$.
Thus, we are able specify the product $\Delta\delta\boldsymbol{\varepsilon}_G^{hT}\boldsymbol{\sigma}^h$ with the independent stress resultants $\boldsymbol{\sigma}^h = [n^{11}, n^{22}, n^{12}, m^{11}, m^{22}, m^{12}, q^1, q^2]^T$ using (44) - (46)

$$
\begin{aligned}
\Delta\delta\boldsymbol{\varepsilon}_G^{hT}\boldsymbol{\sigma}^h &= \sum_I^4 \sum_K^4 \delta\mathbf{v}_I^T\, \mathbf{k}_{\sigma IK}\, \Delta\mathbf{v}_K \\
&= \sum_I^4 \sum_K^4 \begin{bmatrix} \delta\mathbf{u}_I \\ \delta\boldsymbol{\beta}_I \end{bmatrix}^T \begin{bmatrix} \hat{n}_{IK}\mathbf{1} & (\hat{m}_{IK} + \hat{q}_{IK}^{uw})\mathbf{T}_K \\ (\hat{m}_{IK} + \hat{q}_{IK}^{wu})\mathbf{T}_I^T & \delta_{IK}\, \hat{\mathbf{M}}_I(\mathbf{h}_I) \end{bmatrix} \begin{bmatrix} \Delta\mathbf{u}_K \\ \Delta\boldsymbol{\beta}_K \end{bmatrix}
\end{aligned}
\tag{47}
$$

where $\mathbf{k}_{\sigma IK}$ is determined with

$$
\begin{aligned}
\hat{n}_{IK} &= n^{11}\, N_{I,1}\, N_{K,1} + n^{22}\, N_{I,2}\, N_{K,2} + n^{12}\, (N_{I,1}\, N_{K,2} + N_{I,2}\, N_{K,1}) \\
\hat{m}_{IK} &= m^{11}\, N_{I,1}\, N_{K,1} + m^{22}\, N_{I,2}\, N_{K,2} + m^{12}\, (N_{I,1}\, N_{K,2} + N_{I,2}\, N_{K,1}) \\
\hat{q}_{IK}^{uw} &= \tfrac{1}{2}(q^\xi\, N_{I,\xi}\, f_{IK}^1 + q^\eta\, N_{I,\eta}\, f_{IK}^2) \\
\hat{q}_{IK}^{wu} &= \tfrac{1}{2}(q^\xi\, N_{K,\xi}\, f_{IK}^1 + q^\eta\, N_{K,\eta}\, f_{IK}^2) \\
\hat{\mathbf{M}}_I &= \mathbf{T}_{3I}^T\, \mathbf{H}_I^T\, \mathbf{M}_I(\mathbf{h}_I)\, \mathbf{H}_I\, \mathbf{T}_{3I} \\
\mathbf{h}_I &= m^{11}\, N_{I,1}\, \mathbf{x}_{,1}^h + m^{22}\, N_{I,2}\, \mathbf{x}_{,2}^h + m^{12}\, (N_{I,2}\, \mathbf{x}_{,1}^h + N_{I,1}\, \mathbf{x}_{,2}^h) \\
&\quad + q^\xi\, N_{I,\xi}\, \xi_I \mathbf{x}_{,\xi}^M + q^\eta\, N_{I,\eta}\, \eta_I \mathbf{x}_{,\eta}^L
\end{aligned}
\tag{48}
$$

$$
[f_{IK}^1] = \begin{bmatrix} 1 & 1 & 0 & 0 \\ 1 & 1 & 0 & 0 \\ 0 & 0 & 1 & 1 \\ 0 & 0 & 1 & 1 \end{bmatrix} \qquad [f_{IK}^2] = \begin{bmatrix} 1 & 0 & 0 & 1 \\ 0 & 1 & 1 & 0 \\ 0 & 1 & 1 & 0 \\ 1 & 0 & 0 & 1 \end{bmatrix} \qquad \begin{bmatrix} q^\xi \\ q^\eta \end{bmatrix} = \mathbf{J}^{-T} \begin{bmatrix} q^1 \\ q^2 \end{bmatrix}.
$$

C Stresses and Material Law

We consider a laminate with $NLAY$ layers of total thickness h. Hence the thickness coordinate ξ^3 lies for an arbitrary reference surface in the range $h_u \le \xi^3 \le h_o$. It is assumed that the constitutive behaviour of each layer can be described using a transversal isotropic material law. Thus we use a homogenized material law with averaged stresses for the fiber matrix composite. In the following the subscript G indicates components with respect to the element coordinate system $\mathbf{t}_i$ according to (9), whereas the subscript L denotes tensor components with respect to the orthogonal layer basis $\mathbf{a}_i$

$$\begin{aligned} \mathbf{a}_1 &= c\,\mathbf{t}_1 + s\,\mathbf{t}_2 \\ \mathbf{a}_2 &= -s\,\mathbf{t}_1 + c\,\mathbf{t}_2 \\ \mathbf{a}_3 &= \mathbf{t}_3 \end{aligned} \tag{49}$$

where $c = \cos\varphi$, $s = \sin\varphi$ and $\mathbf{a}_1$ is related to the fiber direction. Introducing the coefficients $T_{ij} = \mathbf{t}_i \cdot \mathbf{a}_j$

$$[T_{ij}] = \begin{bmatrix} c & -s & 0 \\ s & c & 0 \\ 0 & 0 & 1 \end{bmatrix} \tag{50}$$

the transformation of the strain components from the global to the local coordinate system $\tilde{E}_{kl} = T_{ik} E_{ij} T_{jl}$ can be written in matrix notation

$$\begin{bmatrix} \tilde{E}_{11} \\ \tilde{E}_{22} \\ 2\tilde{E}_{12} \\ 2\tilde{E}_{13} \\ 2\tilde{E}_{23} \end{bmatrix} = \begin{bmatrix} c^2 & s^2 & sc & 0 & 0 \\ s^2 & c^2 & -sc & 0 & 0 \\ -2sc & 2sc & c^2 - s^2 & 0 & 0 \\ 0 & 0 & 0 & c & s \\ 0 & 0 & 0 & -s & c \end{bmatrix} \begin{bmatrix} E_{11} \\ E_{22} \\ 2E_{12} \\ 2E_{13} \\ 2E_{23} \end{bmatrix} \tag{51}$$

$$\mathbf{E}_L = \mathbf{T}_k\,\mathbf{E}_G$$

where the index k refers to layer k. The strain energy is an invariant function

$$W_s = \frac{1}{2}\,\mathbf{E}_L^T \mathbf{C}_L\,\mathbf{E}_L = \frac{1}{2}\,\mathbf{E}_G^T \mathbf{C}_G\,\mathbf{E}_G \tag{52}$$

and yields with (51) the transformation for the symmetric constitutive matrix

$$\mathbf{C}_G = \mathbf{T}_k^T \mathbf{C}_L\,\mathbf{T}_k = \begin{bmatrix} \mathbf{C}_k & \mathbf{0} \\ \mathbf{0} & \tilde{\mathbf{C}}_k \end{bmatrix} \tag{53}$$

with components

$$\begin{aligned} C_{11G} &= c^4 C_{11L} + 2s^2c^2\,(C_{12L} + 2C_{33L}) + s^4 C_{22L} \\ C_{22G} &= s^4 C_{11L} + 2s^2c^2\,(C_{12L} + 2C_{33L}) + c^4 C_{22L} \\ C_{12G} &= s^2c^2\,(C_{11L} + C_{22L} - 4C_{33L}) + (s^4 + c^4)\,C_{12L} \\ C_{13G} &= c^3 s\,(C_{11L} - C_{12L} - 2C_{33L}) + s^3 c\,(C_{12L} - C_{22L} + 2C_{33L}) \\ C_{23G} &= s^3 c\,(C_{11L} - C_{12L} - 2C_{33L}) + c^3 s\,(C_{12L} - C_{22L} + 2C_{33L}) \\ C_{33G} &= s^2c^2\,(C_{11L} + C_{22L} - 2C_{12L} - 2C_{33L}) + (s^4 + c^4)\,C_{33L} \end{aligned} \tag{54}$$

$$\begin{aligned} \tilde{C}_{11G} &= c^2 C_{44L} + s^2 C_{55L} \\ \tilde{C}_{22G} &= s^2 C_{44L} + c^2 C_{55L} \\ \tilde{C}_{12G} &= sc\,(C_{44L} - C_{55L})\,. \end{aligned}$$

The elements of the material matrices of a layer k depend on the elastic constants E_i, G_{ik} and ν_{ik} of a three-dimensional material law with transversal isotropy, see e.g. Tsai [32],

$$\begin{aligned} C_{11L} &= \frac{E_1}{1-\nu_{12}\,\nu_{21}} \\ C_{22L} &= \frac{E_2}{1-\nu_{12}\,\nu_{21}} \\ C_{12L} &= \frac{\nu_{12}E_2}{1-\nu_{12}\,\nu_{21}} \\ C_{33L} &= G_{12} \\ C_{44L} &= \kappa\, G_{12} \\ C_{55L} &= G_{23} = \kappa\,\frac{E_2}{2\,(1+\nu_{23})}\,. \end{aligned} \tag{55}$$

where, κ denotes the shear correction factor. For simplicity we choose only one value, the one for isotropic material behaviour $\kappa = 5/6$. The potential character of the strain energy requires $\nu_{12}/E_1 = \nu_{21}/E_2$. Thus, we consider 5 independent material constants.
Next the relation between the Green-Lagrangian strains at a layer point with coordinate ξ^3 and the shell strains is written in matrix notation

$$\begin{bmatrix} E_{11} \\ E_{22} \\ 2E_{12} \\ 2E_{13} \\ 2E_{23} \end{bmatrix} = \begin{bmatrix} 1 & 0 & 0 & \xi^3 & 0 & 0 & 0 & 0 \\ 0 & 1 & 0 & 0 & \xi^3 & 0 & 0 & 0 \\ 0 & 0 & 1 & 0 & 0 & \xi^3 & 0 & 0 \\ 0 & 0 & 0 & 0 & 0 & 0 & 1 & 0 \\ 0 & 0 & 0 & 0 & 0 & 0 & 0 & 1 \end{bmatrix} \begin{bmatrix} \varepsilon_{11} \\ \varepsilon_{22} \\ 2\varepsilon_{12} \\ \kappa_{11} \\ \kappa_{22} \\ 2\kappa_{12} \\ \gamma_1 \\ \gamma_2 \end{bmatrix} \tag{56}$$

$$\mathbf{E}_G = \mathbf{A}\,\boldsymbol{\varepsilon}$$

We insert the corresponding equation for the virtual strains in the virtual work expression of the body $\delta W^i = \int_\Omega \int_{(\xi^3)} \delta\mathbf{E}_G^T \mathbf{S}_G\,\bar{\mu}\,d\xi^3 d\,\Omega$ with the vector of stresses

$$\mathbf{S}_G = [S^{11}, S^{22}, S^{12}, S^{13}, S^{23}]^T\,, \tag{57}$$

where S^{ij} denote the contravariant components of the Second-Piola Kirchhoff stress tensor and $\bar{\mu}$ is the determinant of the so–called shifter tensor. Since we use an orthogonal basis system at the element center $\bar{\mu} = 1$ holds only at the center. The numerical tests however show that $\bar{\mu} = 1$ can be set for the whole element and convergence against the correct solution is given. Here, the constraint $S^{33} = 0$ is identically enforced. The virtual work expression yields the vector of the stress resultants

$$\partial_{\boldsymbol{\varepsilon}} W = \int_{(h_u)}^{(h_o)} \mathbf{A}^T \mathbf{S}_G\,\bar{\mu}\,d\xi^3 \tag{58}$$

with $\mathbf{S}_G = \mathbf{C}_G\,\mathbf{E}_G$. The linearization considering the kinematic equation (49) yields

$$\mathbf{C} = \partial^2_{\boldsymbol{\varepsilon}} W \;=\; \int_{(h_u)}^{(h_o)} \mathbf{A}^T \frac{\partial \mathbf{S}_G}{\partial \mathbf{E}_G} \frac{\partial \mathbf{E}_G}{\partial \boldsymbol{\varepsilon}}\, \bar{\mu}\; d\xi^3 = \int_{(h_u)}^{(h_o)} \mathbf{A}^T\, \mathbf{C}_G\, \mathbf{A}\, \bar{\mu}\; d\xi^3 \tag{59}$$

where the thickness integration in (51) can be carried out analytically. One obtains for a laminate with $NLAY$ layers

$$\mathbf{C} \;=\; \begin{bmatrix} \mathbf{C}^m & \mathbf{C}^{mb} & \mathbf{0} \\ \mathbf{C}^{mbT} & \mathbf{C}^b & \mathbf{0} \\ \mathbf{0} & \mathbf{0} & \mathbf{C}^s \end{bmatrix}$$

with

$$\begin{aligned} \mathbf{C}^m &= \sum_{k=1}^{NLAY} \mathbf{C}_k\, h_k \\ \mathbf{C}^b &= \sum_{k=1}^{NLAY} \mathbf{C}_k\, [\frac{(h_k)^3}{12} + h_k\, (\xi^3_{sk})^2\,] \\ \mathbf{C}^{mb} &= \sum_{k=1}^{NLAY} \mathbf{C}_k\, h_k\, \xi^3_{sk} \\ \mathbf{C}^s &= \sum_{k=1}^{NLAY} \tilde{\mathbf{C}}_k\, h_k\,. \end{aligned} \tag{60}$$

In (60) h_k is the thickness of the k-th layer, ξ^3_{sk} is the distance from the midpoint of the considered layer to the reference surface. As can be seen the material law is characterized by the well known coupling effect between membrane and bending terms. Finally from (58) we obtain the vector of the stress resultants

$$\partial_{\boldsymbol{\varepsilon}} W = \mathbf{C}\,\boldsymbol{\varepsilon}\,. \tag{61}$$

It is important to note that in the Hu–Washizu functional (1) the independent strains $\boldsymbol{\varepsilon}$ enter into the constitutive model, and thus in (61).

D Effective elimination of the stress and strain parameters

Due to the orthogonality of the interpolation functions $\mathbf{N}_\sigma$ and $\mathbf{N}^2_\varepsilon$ one obtains

$$\mathbf{F} = \int_{(\Omega_e)} \begin{bmatrix} \mathbf{N}^1_\varepsilon \\ \mathbf{N}^2_\varepsilon \end{bmatrix}^T \mathbf{N}_\sigma dA = \begin{bmatrix} \mathbf{F}_1 \\ \mathbf{0} \end{bmatrix} \qquad \mathbf{F}_1 = \begin{bmatrix} A_e\, \mathbf{1}_8 & \mathbf{0} \\ \mathbf{0} & \mathbf{f} \end{bmatrix} \qquad \mathbf{f}_{(6\times 6)} = \begin{bmatrix} \mathbf{f}^m & \mathbf{0} & \mathbf{0} \\ \mathbf{0} & \mathbf{f}^b & \mathbf{0} \\ \mathbf{0} & \mathbf{0} & \mathbf{f}^s \end{bmatrix}. \tag{62}$$

Using an approximation for j the submatrices in $\mathbf{f}$ can be integrated analytically, see Ref. [16].
It is not necessary to perform the double inversion in $\hat{\mathbf{H}} = (\mathbf{F}^T\mathbf{H}^{-1}\mathbf{F})^{-1}$. After some algebraic manipulations considering (62) one obtains

$$\hat{\mathbf{H}} = (\mathbf{F}^T\mathbf{H}^{-1}\mathbf{F})^{-1} = \mathbf{F}_1^{-1}\,\bar{\mathbf{H}}_{11}\,\mathbf{F}_1^{-T} \tag{63}$$

Here, $\bar{\mathbf{H}}_{11}$ is the result of a static condensation applied to the following linear system of equations

$$\begin{bmatrix} \mathbf{H}_{11} & \mathbf{H}_{12} \\ \mathbf{H}_{21} & \mathbf{H}_{22} \end{bmatrix} \begin{bmatrix} \mathbf{X}_1 \\ \mathbf{X}_2 \end{bmatrix} = \begin{bmatrix} \mathbf{f}_1^e \\ \mathbf{f}_2^e \end{bmatrix} \tag{64}$$

with $\mathbf{H}_{\alpha\beta} = \int\limits_{(\Omega_e)} \mathbf{N}_\varepsilon^\alpha \, \mathbf{C} \, \mathbf{N}_\varepsilon^\beta \, dA$, which yields

$$\bar{\mathbf{H}}_{11} \, \mathbf{X}_1 = \bar{\mathbf{f}}_1^e \qquad \bar{\mathbf{H}}_{11} = \mathbf{H}_{11} - \mathbf{H}_{12} \, \mathbf{H}_{22}^{-1} \, \mathbf{H}_{21} \qquad \bar{\mathbf{f}}_1^e = \mathbf{f}_1^e - \mathbf{H}_{12} \mathbf{H}_{22}^{-1} \, \mathbf{f}_2^e \tag{65}$$

where the condensed matrices are obtained within a Gauss elimination procedure, see Ref. [33].
Furthermore, using (62) and (65) the matrix product $\hat{\mathbf{H}} \, \mathbf{F}^T \, \mathbf{H}^{-1} \, \mathbf{f}^e$ can be reduced as follows

$$\hat{\mathbf{H}} \, \mathbf{F}^T \mathbf{H}^{-1} \mathbf{f}^e = \mathbf{F}_1^{-1} \, \bar{\mathbf{f}}_1^e \tag{66}$$

Finally we obtain the increment of the strain parameters $\Delta\hat{\boldsymbol{\varepsilon}} = [\Delta\hat{\boldsymbol{\varepsilon}}_1, \Delta\hat{\boldsymbol{\varepsilon}}_2]^T$ as follows. Considering $(27)_3$ and (62) it holds $(\mathbf{f}^s + \mathbf{G} \, \Delta\mathbf{v}) = \mathbf{F}^T \, \Delta\hat{\boldsymbol{\varepsilon}} = \mathbf{F}_1^T \, \Delta\hat{\boldsymbol{\varepsilon}}_1$ and thus

$$\Delta\hat{\boldsymbol{\varepsilon}}_1 = \mathbf{F}_1^{-T} \, (\mathbf{f}_s + \mathbf{G} \, \Delta\mathbf{v}) \tag{67}$$

Solving equation $(27)_2$ for $\Delta\hat{\boldsymbol{\varepsilon}}_2$

$$\begin{bmatrix} \mathbf{H}_{11} & \mathbf{H}_{12} \\ \mathbf{H}_{21} & \mathbf{H}_{22} \end{bmatrix} \begin{bmatrix} \Delta\hat{\boldsymbol{\varepsilon}}_1 \\ \Delta\hat{\boldsymbol{\varepsilon}}_2 \end{bmatrix} = \begin{bmatrix} \mathbf{F}_1 \Delta\hat{\boldsymbol{\sigma}} - \mathbf{f}_1^e \\ -\mathbf{f}_2^e \end{bmatrix} \tag{68}$$

yields

$$\Delta\hat{\boldsymbol{\varepsilon}}_2 = \mathbf{H}_{22}^{-1} \, (-\mathbf{f}_2^e - \mathbf{H}_{21} \, \Delta\hat{\boldsymbol{\varepsilon}}_1) \, , \tag{69}$$

as result of the back-substitution with $-\mathbf{f}_2^e$ and $\Delta\hat{\boldsymbol{\varepsilon}}_1$, thus completing the Gauss elimination procedure, see Ref. [33]. Summarizing, besides the condensation of four parameters the only inverse matrix which has to be computed is $\mathbf{F}_1^{-1}$, which means little effort due to its diagonal structure.

References

[1] Dorninger K, Rammerstorfer FG (1990) A Layered Composite Shell Element for Elastic and Thermoelastic Stress and Stability Analysis at Large Deformations, Int. Num. Meth. Engng. 30: 833–858. 1

[2] Koiter WT (1966) On the nonlinear theory of thin elastic shells, Proc. Kon. Ned. Ak. Wet. B69: 1-54. 1

[3] Ahmad S, Irons BM, Zienkiewicz OC (1970) Analysis of thick and thin shell structures by curved finite elements, Int. J. Num. Meth. Engng. 2: 419–451. 1

[4] Stanley GM, Park KC, Hughes TJR (1986) Continuum–Based Resultant Shell Elements, in: Finite Element Methods for Plate and Shell Structures 1: Element Technology, eds. T.J.R. Hughes and E. Hinton, Swansea U.K.: Pineridge Press. 1

[5] Zienkiewicz OC, Taylor RL, Too J (1971) Reduced integration techniques in general analysis of plates and shells, Int. J. Num. Meth. Engng. 3: 275–290. 1

[6] Belytschko T, Tsay C-S (1983) A stabilization procedure for the quadrilateral plate element with one–point quadrature, Int. J. Num. Meth. Engng. 19: 405–419. 1

[7] Liu WK, Law SE, Lam D, Belytschko T (1986) Resultant–stress degenerated shell element, Comp. Meth. Appl. Mech. Engrg. 55: 261–300. 1

[8] Belytschko T, Leviathan I (1994) Physical stabilization of the 4–node shell element with one point quadrature, Comp. Meth. Appl. Mech. Engrg. 113: 321–350. 1

[9] Simo JC, Rifai MS (1990) A class of mixed assumed strain methods and the method of incompatible modes, Int. J. Num. Meth. Engng. 29: 1595–1638. 1, 3.3

[10] Betsch P, Gruttmann F, Stein E (1996) A 4–node finite shell element for the implementation of general hyperelastic 3d–elasticity at finite strains, Comp. Meth. Appl. Mech. Engrg. 130: 57–79. 1

[11] MacNeal RH (1978) A simple quadrilateral shell element, Computers & Structures 8: 175–183. 1

[12] Hughes TJR, Tezduyar TE (1981) Finite elements based upon Mindlin plate theory, with particular reference to the 4–node bilinear isoparametric element, J. Appl. Mech. 48: 587–595. 1

[13] Dvorkin E, Bathe K-J (1984) A continuum mechanics based four node shell element for general nonlinear analysis, Engineering Computations 1: 77–88. 1, 3.1

[14] Bathe K-J, Dvorkin E (1985) A 4–Node Plate bending element based on Mindlin/Reissner theory and a mixed interpolation, Int. J. Num. Meth. Engng. 21: 367–383. 1

[15] Gruttmann F, Wagner W, Wriggers P (1992) A Nonlinear Quadrilateral Shell Element with Drilling Degrees of Freedom, Arch. Appl. Mech. 62: 474–486. 1

[16] Wagner W, Gruttmann, F (2004) A robust nonlinear mixed hybrid quadrilateral shell element, Int. J. Num. Meth. Engng., in press. 1, 3.2, D

[17] Hughes TJR (1987) The Finite Element Method, Linear static and Dynamic Finite Element Analysis, Prentice–Hall, Inc., Englewood Cliffs, New Jersey. 3.1

[18] Gruttmann F, Wagner W (2004) A stabilized one–point integrated quadrilateral Reissner–Mindlin plate element, Int. J. Num. Meth. Engng. 61: 2273–2295. 3.1

[19] Simo JC, Fox DD, Rifai MS (1989) On a stress resultant geometrically exact shell model. Part II: The linear theory; Computational aspects, Comp. Meth. Appl. Mech. Engrg. 73: 53–92. 3.2

[20] Pian THH, Sumihara K (1984) Rational approach for assumed stress finite elements, Int. J. Num. Meth. Engng. 20: 1685-1695. 3.2

[21] Piltner R, Taylor RL (1999) A systematic construction of B–bar functions for linear and non-linear mixed–enhanced finite elements for plane elasticity problems, Int. J. Num. Meth. Engng. 44: 615–639. 3.3

[22] Kasper EP, Taylor RL (2000) A mixed-enhanced strain method part i: Geometrically linear problems, Comput. & Struct. 75: 237–250. 3.3

[23] Kasper EP, Taylor RL (2000) A mixed-enhanced strain method part ii: Geometrically nonlinear problems, Comput. & Struct. 75: 251–260. 3.3

[24] Gruttmann F, Wagner W (2005) A linear quadrilateral shell element with fast stiffness computation, Comp. Meth. Appl. Mech. Engrg. 194: 4279-4300. 3.4

[25] Hughes TJR, Liu WK (1981) Nonlinear finite element analysis of shells: Part I. Three dimensional shells, Comp. Meth. Appl. Mech. Engrg. 26: 331–362. 3.4

[26] Simo JC (1993) On a stress resultant geometrically exact shell model. Part VII: Shell intersections with 5/6-DOF finite element formulations, Comp. Meth. Appl. Mech. Engrg. 108: 319–339. 3.4

[27] Zienkiewicz OC, Taylor RL (2000) The Finite Element Method, Vol.1–3, 5. ed., Butterworth-Heinemann, Oxford. 4

[28] MacNeal RH, Harder RL (1985) A proposed standard set of problems to test finite element accuracy, Finite Elements in Analysis and Design 1: 3–20. 4.1

[29] Basar Y, Montag U, Ding Y (1993) On an isoparametric finite–element for composite laminates with finite rotations, Computational Mechanics 12: 329–348. 4.2, 4.3

[30] Wagner W, Gruttmann F (1994) A simple finite rotation formulation for composite shell elements, Engineering Computations 11: 145–176. 4.2, 4.2, 1, 3, 4.3

[31] Gruttmann F, Sauer R, Wagner W (2000) Theory and Numerics of Three–Dimensional Beams with Elastoplastic Material Behaviour, Int. J. Num. Meth. Engng. 48: 1675–1702. A, B

[32] Tsai WS (1988) Composites Design, Think Composites, Dayton. C

[33] Cook RD, Malkus DS, Plesha ME (1989) Concepts and Applications of Finite Element Analysis, John Wiley & Sons, New York, D, D

[34] Abramovich H, Grunwald A, Pevsner P, Weller T, David A, Ghilai G, Green A and Pekker N (2003) Experiments on Axial Compression Postbuckling Behavior of Stiffened Cylindrical Composite Panels, Proceeding of 44_th AIAA/ASME/ASCE/AHS Structures, Structural Dynamics and Material Conference, Norfolk, VI, USA, AIAA paper No. 2003-1793. 4.4

[35] Abramovich H, Grunwald A and Weller T (2003) Improved Postbuckling Simulation for Design of Fibre Composite Stiffened Fuselage Structures- POSICOSS- Part 1 - Test results, TAE Report No. 990, January 2003. 4.4

[36] Wagner W, Wriggers P (1988) A Simple Method for the Calculation of Postcritical Branches, Engineering Computations 5: 103–109. 4.4

[37] Hilber HM, Hughes TJR and Taylor RL (1977) Improved numerical dissipation for time integration algorithms in structural dynamics. Earthquake engineering and structural dynamics 5: 283—292. 4.4